 CMC, vol.19, no.1, pp.57-104, 2010

The Molecular Dynamic Finite Element Method (MDFEM)

Lutz Nasdala[1], **Andreas Kempe**[1] **and Raimund Rolfes**[1]

Abstract: In order to understand the underlying mechanisms of inelastic material behavior and nonlinear surface interactions, which can be observed on macroscale as damping, softening, fracture, delamination, frictional contact etc., it is necessary to examine the molecular scale. Force fields can be applied to simulate the rearrangement of chemical and physical bonds. However, a simulation of the atomic interactions is very costly so that classical molecular dynamics (MD) is restricted to structures containing a low number of atoms such as carbon nanotubes. The objective of this paper is to show how MD simulations can be integrated into the finite element method (FEM) which is used to simulate engineering structures such as an aircraft panel or a vehicle chassis. A new type of finite element is required for force fields that include multi-body potentials. These elements take into account not only bond stretch but also bending, torsion and inversion without using rotational degrees of freedom. Since natural lengths and angles are implemented as intrinsic material parameters, the developed molecular dynamic finite element method (MDFEM) starts with a conformational analysis. By means of carbon nanotubes and elastomeric material it is demonstrated that this pre-step is needed to find an equilibrium configuration before the structure can be deformed in a succeeding loading step.

Keywords: Force fields, molecular dynamic finite element method (MDFEM), carbon nanotubes, elastomeric material, particle mechanics, continuum mechanics.

1 Introduction

A common question that arises at the beginning of a numerical simulation is how to capture relevant effects while keeping the numerical effort as low as possible: Can the material be treated as homogeneous and isotropic, or is it necessary to consider each individual atom? Cracks in materials which might be observed as a result of mechanical exposure or aging are usually treated at another analysis level

[1] Institute of Structural Analysis, Leibniz Universität Hannover, 30167 Hannover, Germany.

than buckling phenomena of thin-walled engineering structures like e. g. cooling towers.

A lot of constitutive material models have been developed so far to describe, e. g., softening behavior, hysteresis loops, friction or fatigue. Though many of these models are physically motivated, they are often enriched by rheological, i. e. phenomenological components like dashpot or friction elements in order to account for inelastic effects. Rheological models are suited for efficient simulations. However, in order to provide an explanation for the physical background of material inelasticity, the aforementioned phenomena have to be deduced from the formulation and breaking of chemical and physical bonds.

Fig. 1 gives an overview of different simulation levels starting with the quantum scale up to macroscale. The most complex and detailed level is the quantum scale which is based on the Schrödinger equation that describes the interactions between electrons, neutrons and protons. The second level is the nanoscale which can be reached by neglecting quantum effects (step 1). Force fields treat atoms as point masses connected by spring elements that represent different bonding types. The mechanical behavior observed in these classical MD simulations can be used as motivation for models on microscale (step 2). For larger structures such as e. g. tires, the results on microscale must be transferred to macroscale which is usually done by homogenization (step 3). Certain problems require the introduction of further simulation levels. For instance, if cracks have to be taken into account, they are often considered by mesoscale models (step 4c). If crack propagation can be neglected (step 4a) or if there are lots of microcracks which can be smeared (step 4b), macroscale models will suffice.

Regardless of the length scale, numerical models can be classified by the simulation technique used, namely particle mechanics or continuum mechanics. In particle mechanics the physical system is treated in a "discrete" way using particles and particle-interactions. From a mathematical point of view particles do not have to be atoms but can be seen in a more general way so that even whole galaxies can be simulated by means of particle mechanics which is based on Newton's second law: The force acting on a body equals the product of mass and acceleration. Particle mechanics is based on force fields which use potentials to describe the interactions between two ore more bodies. The most simple example is Hooke's law for linear springs which is derived from a so-called harmonic potential, a quadratic polynomial. Other well-known examples include the potential for gravitational attraction between objects with mass, the Coulomb potential for electrostatic forces, or van der Waals-bonds and hydrogen bonds that are often analyzed by using the potential of Lennard-Jones (1929), a universal approach that considers both attraction and repulsion forces.

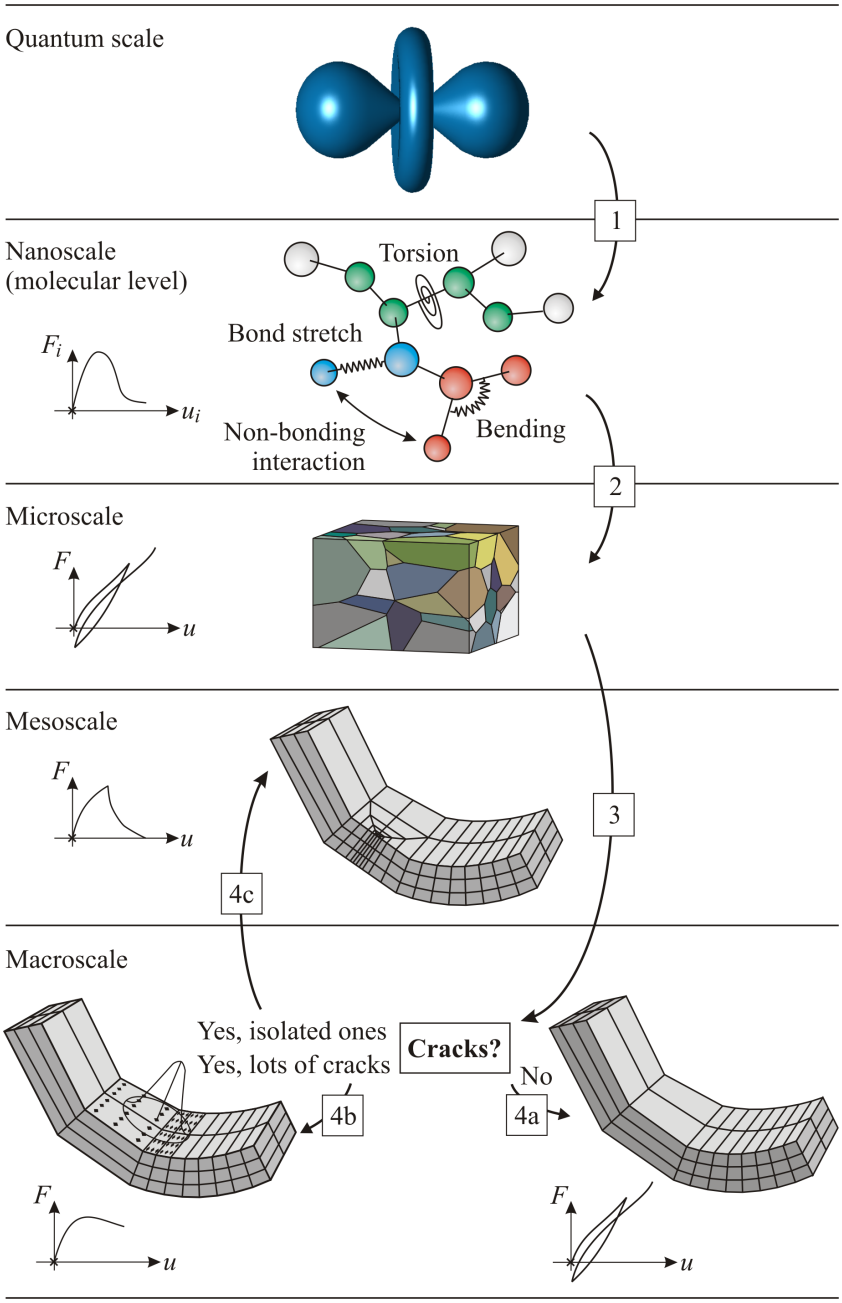

Figure 1: Simulation models at different length scales

Simulations based on particle models, especially molecular dynamic simulations, are usually very expensive in terms of computational time. Typical models e. g. to study crystal crack propagation, comprise up to several million particles which at first glance seems to be a lot. However, compared to one cubic meter gas at a temperature of 273.15 kelvin and a hydrostatic pressure of $p_n = 101.325$ kilopascal which contains $N_L = 2.686763 \cdot 10^{25}\,m^{-3}$ molecules (the Loschmidt constant) or compared to 12 gram of the carbon isotop C_{12} which consists of $N_A = 6.0221367 \cdot 10^{23}\,mol^{-1}$ atoms (the Avogadro constant) or compared to the 200 billion stars comprising milky way, it is obvious that not all problems can be handled by particle mechanics.

For homogeneous structures, continuum mechanical approaches can be applied which are capable of simulating engineering structures like bridges, airplanes, cars etc. However, a simple question of how to explain crack propagation exceeds the capabilities of both particle and continuum mechanics, so that concurrent multi-scale simulations are necessary.

A common approach to link a discrete atomic structure to a continuum region is to apply the Cauchy-Born hypothesis which goes back to Born and Huang (1954) and Ericksen (1984): The bond distance vector $\mathbf{r} = \mathbf{F}\mathbf{r}_0$ in the deformed configuration can be mapped from the bond distance vector $\mathbf{r}_0$ in the undeformed configuration by the deformation gradient tensor $\mathbf{F}$. $\mathbf{F}$ can be decomposed into a stretch and a rotation part, so that the bond length $|\mathbf{r}|$ can be given in terms of the right Cauchy-Green strain tensor. It should be noted that the Cauchy-Born rule involves an approximation because according to the continuum mechanics framework, line elements mapped by $\mathbf{F}$ from the undeformed to the deformed configuration must be infinitesimally small. Bond vectors, however, are of finite length. In order to overcome stability problems, unrealistic wave reflections and other numerical problems resulting from the transition region, various alternative formulations can be found in the literature like the exponential Cauchy-Born rule proposed by Arroyo and Belytschko (2002).

Among different solution techniques that can be applied to a continuum region, the finite element method (FEM) is the most versatile and widespread approach. Due to its very broad range of applications it has become the dominating engineering simulation method. This leads to the desire to also integrate molecular dynamic (MD) simulations to the well-established FEM framework. As shown by Nasdala and Ernst (2005) by the example of the Dreiding force field proposed by Mayo, Olafson, and Goddard (III) (1990), the "molecular dynamic finite element method" (MDFEM) requires special finite elements if multi-body potentials have to be considered.

This paper is addressed to users of finite element codes who want to learn more

about MDFEM, its background in molecular mechanics, the new class of finite elements needed to obtain the same results as traditional MD software, applicable time integration schemes and other implementation issues.

Two examples are provided. In order to demonstrate the robustness and reliability of MDFEM even for geometrically highly nonlinear problems, the first example is about carbon nanotubes with Stone-Wales defects that buckle when subjected to torsional loads. The second example illustrates the benefits for computational material scientists. It is shown that inelastic material behavior can be deduced from the rearrangement of bonds which makes the use of rheological elements obsolete.

2 Chemical and physical bonds

For a better understanding of MDFEM, particularly concerning the numerical effort, a brief overview of the different bond types is given in this chapter. There are two main classes:

- Chemical bonds, the so-called strong bonds:

  The three types of chemical bonds are ionic bonds, covalent bonds and metallic bonds. The electrons of an atom's outermost orbital are called valence electrons. With the exception of the noble gases whose atoms' outer electron shells are completely filled, each atom tries to obtain a noble gas configuration by either gaining or losing valence electrons, depending on its electronegativity. The electronegativity difference between two atoms of a covalent bond is usually less than 1.7 eV. When the difference is 1.7 eV or greater, the bond is predominantly ionic. In a metallic bond, valence electrons are free to move through the crystalline lattice.

- Physical bonds or interactions, which are often referred to as weak bonds:

  The range of weak bondings comprises dipole-dipole interactions, dipole-ion interactions, van der Waals interactions and hydrogen bondings. The distinction between these categories is ambiguous, e. g. hydrogen bondings are often considered to be a special case of van der Waals bonds.

The term "orbital" refers to a mathematical function that describes the probability of an electron's position. The first and simplest one is a sphere and is denoted as s-orbital. It is followed by the p-orbital which has the shape of a dumbbell. Further examples include the d-orbital and the f-orbital.

From an energetic point of view, the overlap of the orbitals must be as large as possible. As shown in Fig. 2, one s-orbital can mix with one, two or three p-orbitals

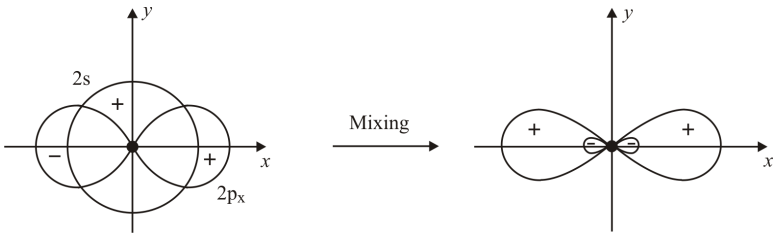

(a) One s-orbital and one p-orbital combined to two sp^1-hybrid orbitals

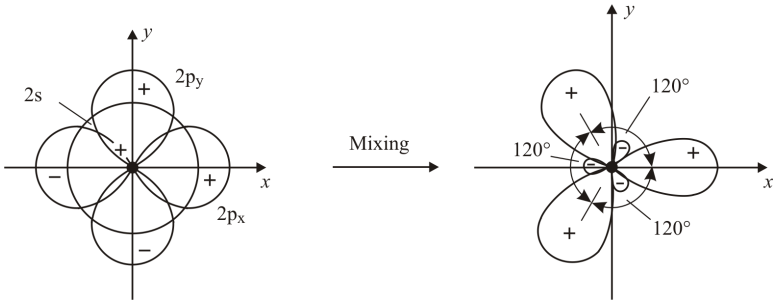

(b) One s-orbital and two p-orbitals combined to three sp^2-hybrid orbitals

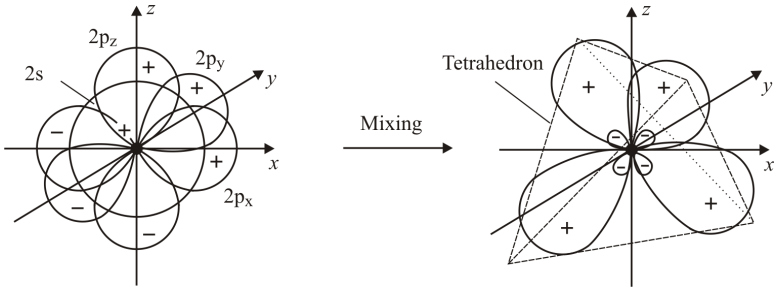

(c) One s-orbital and three p-orbitals combined to four sp^3-hybrid orbitals

Figure 2: Orbital hybridizations of the second shell

to form so-called hybrid orbitals. While the two sp^1-hybrid orbitals are located on a straight line, the three sp^2-hybrid orbitals are in a plane at an included angle of 120°. Between the four energetically equivalent sp^3-hybrid orbitals, which are also referred to as q-orbitals, there is a tetrahedral angle of 109.5°. For the chemical element carbon, all three types are possible: The two carbon atoms of acetylene are sp^1 hybridized, the carbon atoms of graphite have sp^2-hybrid orbitals, and to achieve the high strength of diamond, carbon must be sp^3 hybridized.

2.1 Covalent bonding

A covalent bond can be formed by two atoms of the same kind as well as by different types of atoms. In contrast to ionic bonds, the electrons are not transferred completely but shared pairwise between the participating atoms. The overlapping atomic orbitals form joint electron clouds, the so-called molecular orbitals. Since they provide more space for the electrons, according to Heisenberg's uncertainty relation, molecular orbitals have a smaller impulse and therefore also a lower kinetic energy than the individual atomic orbitals.

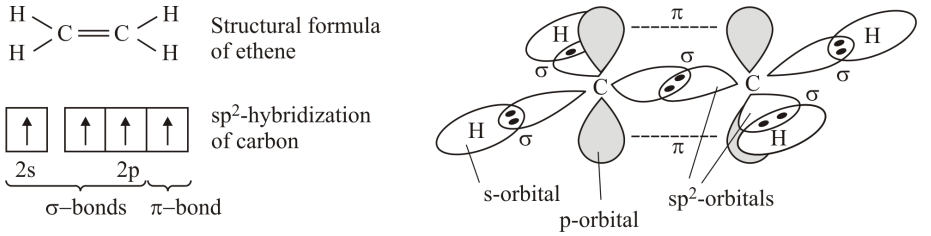

(a) Ethene, C_2H_4

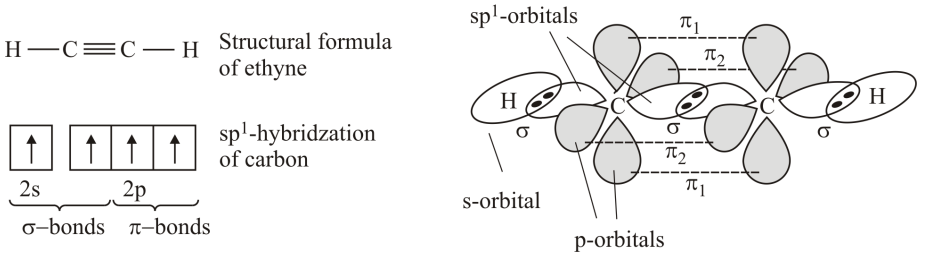

(b) Ethyne, C_2H_2

Figure 3: Double and triple bonds composed of σ- and π-bonds

If two s-orbitals or an s-orbital and a hybrid orbital are involved, we speak of a σ-bond. Each atom contributes one of its valence electrons to the common bond cloud. Diamond owes its high hardness to the fact that each of its carbon atoms forms four σ-bonds which are very strong due to the low kinetic energy. The interaction between two aligned p-orbitals is called π-bond.

While single bonds such as as the hydrogen-carbon bond are σ-bonds, the valence electrons of double and triple bonds are also connected by one or two π-bonds. Fig. 3 shows ethene (ethylene), a main component of many elastomeric materials, which has a double bond, and ethyne where each atom has to share three of its valence electrons. Multiple bonds are not very stable.

2.2 Ionic bonding

When atoms have a large difference in electronegativity, one or more electrons can be completely transferred from the atom with distinct metallic properties to the atom with nonmetallic properties. This process results in a positively charged ion and a negatively charged ion being attracted to each other by electrostatic forces. A typical feature of ionic bonds is the formation of regular ionic crystals, e. g. sodium chloride, commonly known as table salt NaCl.

2.3 Metallic bonding

In a metallic bond, the atoms are organized in a regular crystalline structure. In contrast to the previously introduced valence bonds, the electrons are no longer assigned to specific atoms. Instead, valence electrons separate from the atoms, which then become positively charged metallic ions, while the electrons can move freely and randomly through the crystalline lattice. This "electron gas" accounts for the high electrical and thermal conductivity of metals.

2.4 Van der Waals bonding

The type of bonding that is named after the physicist Johannes Diderik van der Waals (1837-1923) describes the electrostatic interaction between dipoles. As shown in Fig. 4, dipoles are caused by an uneven distribution of electron density within atoms or molecules. As a consequence, there is an offset between the center of mass of all electrons and the protons' center of mass, so that partial charges evolve. Opposite partial charges attract each other whereas equal partial charges repel. Depending on the electronegativity, some compounds have a permanent dipole while other molecules are initially non-polar. When such non-polar molecules approach a dipole, they become dipoles themselves, so-called induced dipoles.

Even if two non-polar atoms or molecules approach one another, they can induce dipoles. The constant fluctuation of the electrons in a non-polar molecule evokes a momentary dipole for a short amount of time which may then polarize a neighboring molecule. These types of van der Waals bondings are often referred to as London dispersion forces and temporary dipoles as the electrical charges are oscillating back and forth.

Compared to an intramolecular force of a covalent or ionic bond, each van der Waals interaction is very weak and only significant when two atoms come close to one another. However, as an intermolecular force, van der Waals bondings can act simultaneously in various directions. Long hydrocarbon chains which can be found in fats and oils as well as in elastomers and polymers owe their elasticity and strength to the collective action of lots of van der Waals forces. They are

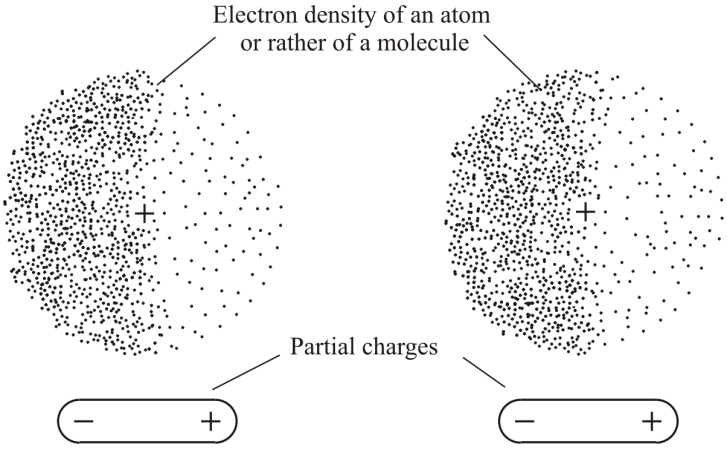

Figure 4: Van der Waals interaction (dipole-dipole interaction)

responsible also for many other chemical properties such as the high boiling point of fats or the fact that even noble gas atoms unite as noble gas crystals - but only at very low temperatures. Van der Waals-interactions are the only linkage between the different walls of a multi-walled carbon nanotube, see e. g. Xie, X.Han, and Long (2007) and Xie and Long (2006).

When the kinetic energy increases, the probability that atoms approach one another decreases. Hence, van der Waals bondings tend to break with rising temperatures. This kind of bond degradation often comes along with a phase transition from the solid to the liquid state or from the liquid to the gaseous state.

2.5 Hydrogen bonding

Hydrogen bonding can be regarded as a special and important case of van der Waals bonding. When a hydrogen atom is covalently bonded to a strong electronegative atom, such as fluorine, oxygen or nitrogen, very strong permanent dipoles arise because each hydrogen atom contains only one proton and therefore cannot attract the joint electron pair very well. As the hydrogen atom has a large positive partial charge, it can now form hydrogen bonds to other molecules with negative partial charges.

The part which provides the hydrogen atom is called donor while the other part is the acceptor. Examples of H-donors include $-\mathrm{OH}$, $-\mathrm{NH_2}$ or $-\mathrm{COOH}$. Typical H-acceptors are compounds that contain oxygen or nitrogen atoms. Hydrogen bonds are considerably strong physical bondings. For this reason water is a very stable compound.

3 From quantum to molecular mechanics

In the last section, different types of bonds have been introduced, however, without quantifying how strong they really are or how the equilibrium distances and angles between the individual atoms can be predicted. In theory, the exact behavior of all chemical and physical bonds can be computed with the help of the famous Schrödinger equation formulated by Erwin Schrödinger (1926). It is the central equation of quantum mechanics, as it describes the interactions between the electrons and the atomic nuclei accurately. An exact solution is available as of today only for the hydrogen atom. Therefore, a variety of approximation procedures has been developed. The range extends from ab initio methods over semi-empirical models up to classical molecular dynamics. A large body of literature exists on this topic, see e. g. Levine (1991), Pauling and Wilson Jr. (1985), and Shen and Atluri (2004). The most important methods will be discussed subsequently.

3.1 Schrödinger wave equation

A time-depended and a time-independent version of the Schrödinger wave equation have been derived. For a system that consists of K nuclei and N electrons, the general time-depended Schrödinger equation reads

$$\hat{E}\Psi(\mathbf{R},\mathbf{r},t) = \hat{H}\Psi(\mathbf{R},\mathbf{r},t) \tag{1}$$

with the energy operator

$$\hat{E} = i\hbar\frac{\partial}{\partial t} \tag{2}$$

and the Hamilton operator, the Hamiltonian

$$\begin{aligned}\hat{H}(\mathbf{R},\mathbf{r}) = &\underbrace{\frac{e^2}{4\pi\varepsilon_0}\sum_{k=j+1}^{N}\sum_{j=1}^{N}\frac{1}{|\mathbf{r}_k-\mathbf{r}_j|}}_{=\hat{V}_\mathrm{e}} \underbrace{-\frac{e^2}{4\pi\varepsilon_0}\sum_{k=1}^{K}\sum_{j=1}^{N}\frac{Z_k}{|\mathbf{R}_k-\mathbf{r}_j|}}_{=\hat{V}_\mathrm{eK}} + \\ &+\underbrace{\frac{e^2}{4\pi\varepsilon_0}\sum_{k=j+1}^{K}\sum_{j=1}^{K}\frac{Z_kZ_j}{|\mathbf{R}_k-\mathbf{R}_j|}}_{=\hat{V}_\mathrm{K}} \underbrace{-\frac{\hbar^2}{2m_\mathrm{e}}\sum_{j=1}^{N}\Delta_{\mathbf{r}_j}}_{=\hat{T}_\mathrm{e}} \underbrace{-\frac{\hbar^2}{2}\sum_{k=1}^{K}\frac{1}{M_j}\Delta_{\mathbf{R}_j}}_{=\hat{T}_\mathrm{K}} \quad .\end{aligned} \tag{3}$$

As solution of the general time-dependent Schrödinger equation, the state function $\Psi(\mathbf{R},\mathbf{r},t)$ depends on the coordinate vectors $\mathbf{R} = (\mathbf{R}_1,\mathbf{R}_2,\ldots,\mathbf{R}_K)$ and $\mathbf{r} = (\mathbf{r}_1,\mathbf{r}_2,\ldots,\mathbf{r}_N)$ of nuclei and electrons as well as on the time t and yields, according to Heisenberg's uncertainty principle, probability distributions of the location and

the impulse of these particles. In terms of its structure, the Schrödinger equation can be seen in analogy to an electromagnetic wave as a wave equation. Hence, Ψ is often denoted as wave equation. When neglecting the spin, the external forces acting on the system and relativistic interactions, the Hamiltonian $\hat{H}$ comprises the operators of the Coulomb potentials $\hat{V}_{\mathrm{e}}$, $\hat{V}_{\mathrm{eK}}$ and $\hat{V}_{\mathrm{K}}$ as well as the operators of the kinetic energies $\hat{T}_{\mathrm{e}}$ and $\hat{T}_{\mathrm{K}}$. M_j and Z_j are the masses and charge numbers of the nuclei, m_{e} is the mass of an electron, ε_0 the electric field constant, $i = \sqrt{-1}$ the imaginary unit and $\hbar = \frac{h}{2\pi}$ a natural constant based on Planck's quantum of action h. The Laplace operators $\Delta_{\mathbf{R}_j} = \frac{\partial^2}{\partial R_{j,x}^2} + \frac{\partial^2}{\partial R_{j,y}^2} + \frac{\partial^2}{\partial R_{j,z}^2}$ and $\Delta_{\mathbf{r}_j} = \frac{\partial^2}{\partial r_{j,x}^2} + \frac{\partial^2}{\partial r_{j,y}^2} + \frac{\partial^2}{\partial r_{j,z}^2}$ indicate that the kinetic energies depend on the curvature of the wave equation.

For reasons of simplicity, the Hamiltonian $\hat{H}$ in Eq. 3 has been assumed to be independent of time t. In this case, a decoupling of the state function

$$\Psi(\mathbf{R},\mathbf{r},t) = \psi(\mathbf{R},\mathbf{r}) \cdot f(t) \tag{4}$$

into a time-independent part $\psi(\mathbf{R},\mathbf{r})$ and a time-dependent part $f(t)$ is possible. Substitution into Eq. 1 yields

$$\psi(\mathbf{R},\mathbf{r}) \cdot \hat{E} f(t) = f(t) \cdot \hat{H}\psi(\mathbf{R},\mathbf{r}) \quad . \tag{5}$$

After division by $f(t) \neq 0$ and using

$$E = \frac{\hat{E} f(t)}{f(t)} \tag{6}$$

we obtain the stationary Schrödinger equation

$$\hat{H}\psi(\mathbf{R},\mathbf{r}) = E\psi(\mathbf{R},\mathbf{r}) \tag{7}$$

which is easier to solve. E is in contrast to $\hat{E}$ not an operator but a simple number. The total energy of the solution

$$E_{\mathrm{tot}} = i\hbar \frac{1}{f(t)} \frac{\partial f(t)}{\partial t} \tag{8}$$

is both space- and time-dependent.

Although the stationary Schrödinger equation given in Eq. 7 is not time-dependent, this does not imply that only static problems can be solved. It just means that the time-dependence of the solutions is known. After multiplication with $f(t)$, Eq. 8 represents a first order differential equation. Its solution

$$f(t) = c \exp\left(-\frac{iE_{\mathrm{tot}}t}{\hbar}\right) \tag{9}$$

yields the temporal evolution of the wave equation, simple sine or cosine oscillations.

An important feature of the Schrödinger equation is that new solutions can be obtained by superposition, which is a typical property of wave equations. For the time-dependent Schrödinger equation, Eq. 1, the general solution approach for ψ and its corresponding complex conjugate ψ^* is given by

$$\Psi(\mathbf{R},\mathbf{r},t) = \sum_n c_n \exp\left(-\frac{iE_n t}{\hbar}\right) \psi_n(\mathbf{R},\mathbf{r}) \tag{10}$$

with

$$c_n = \int \psi_n^*(\mathbf{R},\mathbf{r})\,\Psi(\mathbf{R},\mathbf{r},0)\,d\mathbf{R}\,d\mathbf{r} \quad . \tag{11}$$

To obtain a unique solution, initial conditions have to be defined.

3.2 Ab initio molecular dynamics

Between both extremes, pure ab initio methods on the one hand, which can be used to solve the Schrödinger equation for hydrogen exactly, and classical molecular dynamics on the other hand, where atoms are treated as point masses, a variety of different approaches exists. In order to distinguish themselves from "empirical" classical molecular dynamics, many methods claim to be an "ab initio" approach. As different notations and ratings can be found in the literature, for non-physicists, an evaluation of these methods can be quite challenging. The same approach can be denoted as "quantum mechanical method" by some authors, while others prefer to write "semi-empirical method". Additional information on "ab initio methods" can be found in Marx and Hutter (2000).

3.2.1 Born-Oppenheimer approximation

A basic simplification of the Schrödinger equation which is named after Max Born and Julius Robert Oppenheimer is to separate the equations of motion with regard to the electrons and the nuclei. It exploits the fact that electrons have a much lower mass and move faster that the nuclei, which allows for an immediate adaption to new nuclei positions. The Schrödinger equation of the nuclei is replaced by Newton's equation of motion. The remaining part is called the electronic Schrödinger equation.

Hence, with the help of the Born-Oppenheimer approximation, the Schrödinger equation can be reduced to a many-electron problem. To solve this problem, further approximations such as the Hartree-Fock approach (HF) or the density functional theory (DFT) are necessary.

3.2.2 Hartree-Fock theory

The approach developed by Hartree (1928, 1932) and Fock (1930) reduces the many-electron problem to coupled one-electron problems. The electron-electron interaction terms are replaced by an averaged potential for each electron considering the average potential of the other electrons. On the other hand, the neglect of electron correlation effects is the main source of error of the HF method.

The HF method is comparable to the Ritz approach. In order to determine the Hamiltonian's ground state, trial functions within the framework of a variational principle are introduced. A possible choice of test functions are the so-called Slater determinants Slater, Wilson, and Wood (1969) of one-electron wave equations.

3.2.3 Density functional theory

The density functional theory is based on a publication by Hohenberg and Kohn (1964). They show that the electron energy in the ground state is not only well-defined by a functional of the wave function but also by a functional of the electron density. On this basis, Kohn and Sham (1965) present the so-called local-density approximation (LDA) which can be used to approximate the electron ground-state energy. In combination with a variational principle for the density functional, this approach finally leads to the one-electron Schrödinger equations, also known as Kohn-Sham equations.

Compared to pure ab initio methods with high numerical effort of order $\mathcal{O}(N^4)$, a reduction to order $\mathcal{O}(N^3)$ can be achieved. Methods based on the DFT approach with a reduced effort of $\mathcal{O}(N^2)$ are Car-Parrinello molecular dynamics and the conjugate gradient method (CG) whereas the latter is considered to be a bit more efficient then the method developed by Car and Parrinello (1985).

3.3 Semi-empirical models

The time-dependent self-consistent field (TDSCF) approximation introduced by Dirac (1930) is based on an estimation of the electron distribution, which is used to determine the potential for each single electron with respect to the remaining electrons. Atomic nuclei are assumed to move according to the rules of classical mechanics. The electron's effective potential is also known as Ehrenfest potential, see Ehrenfest (1927) for details. The computed electron distribution acts as a starting point for a new iteration step, which is repeated until the atomic orbitals are determined with sufficient accuracy.

Originally introduced by Bloch (1928) and revised by Slater and Koster (1954), the tight-binding method is another typical representative of the semi-empirical methods. A linear combination of atomic orbitals (LCAO) allows for a parametriza-

tion of the Hamiltonian such that the total energy and the eigenvalues of the electronic Schrödinger equation can be determined. Interatomic forces are computed by means of the Hellmann-Feynman theorem.

An alternative to semi-empirical methods are the so-called hybrid QM/MD methods. As in a typical multiscale model, only a small portion of the system is treated quantum-mechanically, while for the rest of the system MD simulations based on force fields are carried out.

3.4 Classical molecular dynamics

In classical molecular dynamics, the parameterized potential functions only depend on the nuclei positions. Not having to bother with the electrons, it is possible to simulate the interactions between many thousands or even many millions of atoms. In the following, the equations of motion are given in three different forms, which can be easily transformed into each other.

3.4.1 Newton's equation of motion

For a system of N atoms, the equations of motion, also known as Newton's second law, are given as

$$\mathbf{F}_j = \dot{\mathbf{I}}_j = M_j \ddot{\mathbf{R}}_j = -\nabla_{\mathbf{R}_j} V \quad \text{with} \quad j = 1,\ldots,N \tag{12}$$

with the total empirical potential $V = V(\mathbf{R}_1, \mathbf{R}_2, \ldots, \mathbf{R}_j, \ldots, \mathbf{R}_N)$. $\mathbf{F}_j$, M_j and $\mathbf{R}_j$ denote the inner forces, masses and coordinates of atom j, respectively. $\mathbf{I}_j = M_j \dot{\mathbf{R}}_j$ is the momentum vector.

3.4.2 Lagrange's equation of motion

Using the Lagrangian

$$L = E_{\text{kin}} - V \quad , \tag{13}$$

the Lagrange form of the equations of motion reads

$$\frac{d}{dt}\frac{\partial L}{\partial \dot{\mathbf{R}}_j} - \frac{\partial L}{\partial \mathbf{R}_j} = 0 \quad \text{with} \quad j = 1,\ldots,N \quad . \tag{14}$$

Utilizing the generalized coordinates $(q_1, q_2, q_3, q_4, \ldots) = (R_{1,x}, R_{1,y}, R_{1,z}, R_{2,x}, \ldots)$, it can be written as

$$\frac{d}{dt}\frac{\partial L}{\partial \dot{q}_i} - \frac{\partial L}{\partial q_i} = 0 \quad \text{with} \quad i = 1,\ldots,3N \tag{15}$$

and the kinetic energy

$$E_{\text{kin}} = \sum_{j=1}^{N} M_j \frac{\dot{\mathbf{R}}_j^2}{2} = \sum_{i=1}^{3N} M_i \frac{\dot{q}_i^2}{2} \quad . \tag{16}$$

3.4.3 Hamilton's equation of motion

Hamilton's equations of motion comprise two first-order differential equations

$$\dot{p}_i = -\frac{\partial H}{\partial q_i} \quad \text{and} \quad \dot{q}_i = \frac{\partial H}{\partial p_i} \tag{17}$$

with the Hamilton's principal function

$$H = E_{\text{kin}} + V = -L + \sum_{i=1}^{3N} p_i \dot{q}_i \tag{18}$$

and the generalized momentum

$$p_i = \frac{\partial L}{\partial \dot{q}_i} \tag{19}$$

with $(p_1, p_2, p_3, p_4, \ldots) = (I_{1,x}, I_{1,y}, I_{1,z}, I_{2,x}, \ldots)$. Like the Hamiltonian (Eq. 3), Hamilton's principal function (Eq. 18) consists of both a kinetic energy E_{kin} contribution and a potential energy V contribution.

4 The molecular dynamic finite element method

4.1 Requirements for the finite element method

Since MD simulations do not belong to the standard applications of FEM codes, the user has to make the necessary adjustments. In this section, all aspects of the molecular dynamic finite element method (MDFEM), in particular the differences to traditional MD software, are discussed from a FEM user's point of view.

4.1.1 Force fields

In molecular dynamics, the potential energy which, in the previous chapter, is denoted by the variable V as it is usual in quantum mechanics to avoid confusion with the energy operator, is denoted by the variable E and called force field. Force fields can be derived in two complementary ways:

- from quantum mechanical calculations,
- from experimental work,

see e. g. Ercolessi and Adams (1994). Well-known force field approaches include AMBER (Assisted Model Building with Energy Refinement, see e. g. Weiner and Kollman (1981)), CHARMM (Chemistry at HARvard Molecular Mechanics, see Brooks, Bruccoleri, Olafson, States, Swaminathan, and Karplus (1983)), the "Molecular Mechanics"-force fields MM1, MM2, MM3 and MM4 (Allinger and Chen (1996)), ECEPP (Roterman, Lambert, Gibson, and Scheraga (1989)), and UFF (Universal Force Field, see Rappé, Casewit, Colwell, Goddard (III), and Skiff (1992)).

Main application of classical molecular dynamic simulations is a calculation of equilibrium configurations within a so-called conformational analysis, without considering bond forming and bond rupture reactions, cf. e. g. Schlick (2002). Force field potentials are often extended and adapted in order to account for specific material aspects. The potential by Stillinger and Weber (1985) for instance is well-suited and efficient for the approximation of crystalline silicon as it includes terms to enforce a diamond-like tetrahedral local structure which results in a more stable and realistic than compact structure. For the treatment of non-bonded interactions, the popular potential by Lennard-Jones (1929) is often preferred due to its efficiency, while for example the Buckingham (1938) potential introduces an exponential function of distance to capture the exchange repulsion stemming from the Pauli exclusion principle more precisely. Some approaches make use of the concept of local environment, with bond strengths depending on the bonding environment e. g. the many-body potentials by Tersoff (1988) and Brenner (1990). ReaxFF by van Duin, Dasgupta, Lorant, and Goddard (III) (2001) replaces explicit bonds with bond orders to account for continuous formation and breaking of bonds.

In general, MDFEM can be applied to all kinds of force fields. However, it should be noted that many force fields are designed for a limited range of chemical elements or rather very special substances like proteins or peptides and cannot be used to examine other structures.

4.1.2 Short- and long-range force field potentials

Most chemical and physical bonds can be described using pair potentials. From a numerical point of view, a distinction has to be made between short-range (bonded) and long-range (non-bonded) interactions. In the following, the implications for the finite element method are discussed by the example of the Dreiding force field (Mayo, Olafson, and Goddard (III) (1990)).

The bond stretch between the atoms I and J can be expressed by a linear approach

$$E_{\mathrm{B}}^{\mathrm{lin}} = \frac{1}{2} k_{\mathrm{e}} (R_{IJ} - R_{\mathrm{e}})^2 \tag{20}$$

(parabolic potential) that is well-suited for small deformations. It depends on the natural bond length R_e, the interatomic distance R_{IJ} and the stiffness k_e. To account for nonlinear bending at large deformations, the function derived by Morse (1929)

$$E_B = D_e \left[\exp(-\alpha n(R_{IJ} - R_e)) - 1\right]^2 \quad \text{with} \quad \alpha = \frac{1}{n}\sqrt{\frac{k_e}{2D_e}} \tag{21}$$

is applied. The parameter D_e denotes the fracture energy. n is the bond order, e. g. $n = 1$ for the σ-bonds of diamond, $n = 1.333$ for graphene, $n = 1.5$ for benzene, $n = 2$ for the π-bond of ethene or $n = 3$ for the π-bond of ethyne. The nonlinear Morse approach corresponds to the linear one if deformations are small $R_{IJ} \to R_e$.

Bond stretch can be seen as a quite stable connection between an atom and its closest neighbors. For instance, hydrogen has one neighbor, the carbon atoms of ethyne have two neighboring atoms, and the carbon atoms of graphene are neighbored by 3 atoms. The number of neighboring atoms is limited to 4 which is the case for diamond.

An approach widely used to describe long-range van der Waals interactions is given by Lennard-Jones (1929). The general form reads

$$E^{LJ}_{m,n}(R_{IJ}) = \frac{\varepsilon}{n-m}\left(\frac{n^n}{m^m}\right)^{\frac{1}{n-m}}\left[\left(\frac{\sigma}{R_{IJ}}\right)^n - \left(\frac{\sigma}{R_{IJ}}\right)^m\right] \quad \text{with} \quad m < n \quad . \tag{22}$$

While repulsion forces are expressed by the first term, the second term accounts for attraction forces. ε denotes the size of the forces and σ refers to the zero-crossing of the potential. Often the form $(m,n) = (6,12)$ is applied, whereas $m = 6$ reflects the actual van der Waals force for large distances, and $n = 12$ is chosen for simplicity reasons without a physical motivation. The resulting large repulsion forces avoid that two atoms come too close. Substituting the parameters ε and $\sigma = \sqrt[6]{\frac{1}{2}}R_{e,vdW}$ with the fracture energy $D_{e,vdW}$ and the natural length $R_{e,vdW}$ leads to the (6,12)-form of the Lennard Jones (LJ) potential

$$E^{LJ}_{vdW}(R_{IJ}) = D_{e,vdW}\left[\left(\frac{R_{IJ}}{R_{e,vdW}}\right)^{-12} - 2\left(\frac{R_{IJ}}{R_{e,vdW}}\right)^{-6}\right] \quad . \tag{23}$$

Hydrogen bondings are characterized with the help of a modified Lennard-Jones approach. The general equation 22 is altered by substituting $(m,n) = (10,12)$ and multiplying with $\cos^4\Theta_{DHA}$. The potential function then reads

$$E_{hb}(R_{DA},\Theta_{DHA}) = D_{hb}\left[5\left(\frac{R_{DA}}{R_{hb}}\right)^{-12} - 6\left(\frac{R_{DA}}{R_{hb}}\right)^{-10}\right]\cos^4\Theta_{DHA} \quad . \tag{24}$$

Θ_{DHA} denotes the angle between the donor D, hydrogen H and acceptor A. R_{DA} is the distance between the donor and the acceptor. Both material parameters, the modified fracture energy D_{hb} and the natural equilibrium distance R_{hb}, depend on the hydrogen bridge type and hence have to be fitted to experimental data.

Other force fields often use a simple (10,12)-Lennard-Jones approach

$$E_{\mathrm{hb}}^{\mathrm{LJ}}(R_{\mathrm{DA}}) = D_{\mathrm{hb}} \left[5 \left(\frac{R_{\mathrm{DA}}}{R_{\mathrm{hb}}} \right)^{-12} - 6 \left(\frac{R_{\mathrm{DA}}}{R_{\mathrm{hb}}} \right)^{-10} \right] \tag{25}$$

to describe hydrogen bonding.

Coulomb or electrostatic interactions can be simulated by means of the Coulomb potential

$$E_{\mathrm{Q}}(R_{IJ}) = \frac{1}{4\pi\varepsilon_0} \frac{q_I q_J}{R_{IJ}} \tag{26}$$

for two point loads q_I and q_J with a distance R_{IJ}. ε_0 denotes the dielectric constant. Charges with equal algebraic signs repel whereas opposite charges attract each other.

In contrast to bond stretch, the long-range van der Waals, hydrogen and Coulomb interactions connect an atom to a multitude of atoms. In theory, each atom has a direct connection to all atoms of the same structure. For practical applications, it is recommended to introduce cutoff distances or special algorithms in order to reduce the numerical effort of a MDFEM analysis:

- Since interaction forces approach zero for large distances, bondings that exceed a certain range, e. g. three times the natural length, can be neglected.
- For a geometric nonlinear analysis, the selection should be revised in regular intervals as the interatomic distances are supposed to change.
- For very large structures and e. g. long-range interactions that decay slowly with distance, it is necessary to bundle long-range interactions using special algorithms. For instance, the Ewald summation has been derived for the fast treatment of electrostatic interactions and is often used in biomolecular systems such as proteins and enzymes in a crystalline state, whereas methods based on multipole expansions are often used for non-periodic systems, such as an enzyme in solution. For details, see e. g. Schlick (2002).

For static and implicit dynamic procedures, long-range potentials lead to a very large bandwidth of the stiffness matrix. Therefore, it should be considered to use an explicit time-integration scheme, even if the problem is quasi-static.

4.1.3 Multi-body force field potentials

Sophisticated force field approaches also include multi-body potentials. The simplest example is a three-body potential that considers an energy increase if the angle Θ_{IJK} between two bonds IJ and JK differs from the natural angle Θ_J^0. The resulting deformation mode is called bending. In analogy to the natural lengths introduced in the previous section, the natural angle yields the energy-free equilibrium configuration with regard to bending. For small deformations, the Dreiding force field approach for bending reads

$$E_{\mathrm{A}}^{\mathrm{lin}} = \frac{1}{2} K_{IJK} \left[\Theta_{IJK} - \Theta_J^0\right]^2 \quad . \tag{27}$$

For large deformations, an extended cosine approach

$$E_{\mathrm{A}} = \begin{cases} \frac{1}{2} C_{IJK} \left[\cos\Theta_{IJK} - \cos\Theta_J^0\right]^2 & \text{for} \quad \Theta_j^0 \neq 180^\circ \\ K_{IJK} \left[1 + \cos\Theta_{IJK}\right] & \text{for} \quad \Theta_j^0 = 180^\circ \end{cases} \tag{28}$$

can be used which accounts for additional natural angles.

The Dreiding torsion energy

$$E_{\mathrm{T}} = E_{IJKL} = \frac{1}{2} V_{IJKL} \left[1 - \cos\left[n_{JK}(\varphi - \varphi_{JK}^0)\right]\right] \tag{29}$$

is a function of the dihedral angle $\varphi = \varphi_{IJKL}$ that is defined by the two planes IJK and JKL, the natural angle φ_{JK}^0 and the periodicity n_{JK}. A linearization of Eq. 29 can be carried out in case of small deformations $\varphi \rightarrow \varphi_{JK}^0$. This leads to the torsion energy

$$E_{\mathrm{T}}^{\mathrm{lin}} = \frac{1}{4} V_{IJKL} n_{JK}^2 (\varphi - \varphi_{JK}^0)^2 \quad . \tag{30}$$

As shown in section 4.2, special user elements are required to consider multi-body potentials within the MDFEM framework.

4.1.4 Natural lengths and angles

Instead of studying the behavior of molecules under external loading, MD simulations usually aim to determine minimum energy conformations. In most cases, molecules can be seen as statically overdetermined systems and as such the equilibrium distances and angles of the overall structure usually differ from the natural lengths and angles which are also referred to as constitutive lengths and angles.

In order to utilize force fields in finite element simulations, molecular dynamic finite elements must be able to “memorize” the natural distances and angles with

the help of intrinsic material parameters. As a consequence, in contrast to standard elements, the coordinates of the initial configuration only have to be given approximately.

4.1.5 Linear and nonlinear analysis

It is obvious that the finite element code must be able to consider both geometrical and physical nonlinearities since interatomic bonds and interactions can undergo large motions and rotations leading to bond breakage or rather a rearrangement of bonds.

Nevertheless, it is often desirable to also have the opportunity to perform a linear analysis. As already mentioned and shown in section 4.1.9 in more detail, the equilibrium configuration is generally unknown, even for an unloaded structure. A linear analysis using the harmonic force field potentials can improve the initial configuration at low numerical cost since no iteration is required. Then, the linear force field potentials are exchanged by their nonlinear counterparts and a nonlinear simulation step is performed to finish the conformational analysis.

4.1.6 Material parameters

In structural mechanics, usually comprehensive tests are required to obtain material parameters for sophisticated material models such as a viscoplastic damage model. MDFEM users, however, do not have to worry about expensive and time-consuming testing issues because all the parameters are already provided by the force fields. The different force field approaches can be seen as large databases from which the required parameters can be extracted.

It is recommended to start with a so-called "universal" force field which usually includes the complete range of chemical elements. Force fields developed for special applications such as the analysis of proteins or DNAs may give better results if similar structures are to be examined, but are often limited to a small subset of the periodic table of the chemical elements. Hence, bevor applying a specialized force field, the user has to check whether all chemical elements of his structure are involved.

To evaluate the convergence of the numerical solution, FE solvers use error tolerances which are based either on relative or on absolute values for the displacements and forces. The latter case is inadmissible if SI units are used because, among other reasons, the tolerances would be too high so that false results could be accepted as true. Therefore, a general recommendation is to replace the SI units m, N, kg and s by the following unit system: $\mathrm{nm} = 10^{-9}\,\mathrm{m} = 10\,\text{Ångström}$, $\mathrm{nN} = 10^{-9}\,\mathrm{N}$, $\mathrm{akg} = 1\,\text{atto kg} = 10^{-18}\,\mathrm{kg}$ and $\mathrm{ns} = 10^{-9}\,\mathrm{s}$.

4.1.7 Finite elements without rotational degrees of freedom

In molecular dynamics, atoms are treated as point masses which possess only translational degrees of freedom, implying that only finite elements without rotational degrees of freedom should be used. However, a common approach is to describe the atomic interactions by means of standard beam elements which have rotational degrees of freedom, cf. Wang and Wang (2004), Tserpes and Papanikos (2005), Harik (2002) and Li and Chou (2004). At this point, it must be stressed that beam models can only be regarded as a workaround, being used for simplicity reasons.

As shown in section 4.2, special user elements with the following characteristics have to be introduced:

- To be able to decouple bending and torsion energies, the finite elements must not have rotational degrees of freedom.
- The force field parameters can be applied directly.
- Compared to beam models that use rotational degrees of freedom, only half the number of degrees of freedom is necessary which is much more efficient.

Note that for a beam element model the force field parameters have to be transformed to normal, bending and torsional stiffnesses and strengths. And what is more: It can be shown that the specification of the bending and torsion parameters is ambiguous because even for the pure torsion mode depicted in Fig. 6(e) some beam elements, namely the cantilever beams, are subjected to bending. That means, torsion between the planes of two adjacent atom groups IJK and JKL can be considered both by torsion of the beam JK and by bending of the beams IJ and KL.

4.1.8 Time integration schemes

The equation of motion can be written in the general form

$$\mathbf{R} = \mathbf{M}\ddot{\mathbf{u}} + \mathbf{I} - \mathbf{P} = \mathbf{0} \tag{31}$$

with the residual vector $\mathbf{R}$, the mass matrix $\mathbf{M}$, the acceleration vector $\ddot{\mathbf{u}}$ and the vectors of the internal and external forces $\mathbf{I} = \mathbf{I}(\mathbf{u}, \dot{\mathbf{u}})$ and $\mathbf{P} = \mathbf{P}(\mathbf{u}, \dot{\mathbf{u}})$.

In molecular dynamics, often explicit time integration schemes are applied. Verlet (1967) developed one of the most popular algorithms, which can be derived using a double Taylor series with two time points $t_0 - \Delta t$ and $t_0 + \Delta t$, that is truncated after the cubic term. However, the Verlet algorithm is not available in most finite element codes. In addition, it is unusual to apply multi-step algorithms such as the higher order Runge-Kutta methods. Considering this, we concentrate on the three most important time integration schemes available in commercial finite element codes:

- **The implicit HHT method**

The HHT method is an extension of the implicit time integration scheme developed by Newmark (1959) that is based on a Taylor series expansion of the displacements

$$\mathbf{u}_{n+1} = \mathbf{u}_n + \Delta t\, \dot{\mathbf{u}}_n + \Delta t^2 \left[\left(\frac{1}{2} - \beta \right) \ddot{\mathbf{u}}_n + \beta \ddot{\mathbf{u}}_{n+1} \right] \tag{32}$$

and the velocities

$$\dot{\mathbf{u}}_{n+1} = \dot{\mathbf{u}}_n + \Delta t \left[(1-\gamma)\ddot{\mathbf{u}}_n + \gamma \ddot{\mathbf{u}}_{n+1} \right] \tag{33}$$

where quadratic and higher order terms are approximated by a quadrature rule. After rearranging the equations, we obtain the displacements at time t_{n+1}

$$\dot{\mathbf{u}}_{n+1} = \frac{\gamma}{\beta \Delta t}(\mathbf{u}_{n+1} - \mathbf{u}_n) + \left(1 - \frac{\gamma}{\beta} \right) \dot{\mathbf{u}}_n + \Delta t \left(1 - \frac{\gamma}{2\beta} \right) \ddot{\mathbf{u}}_n \tag{34}$$

and the accelerations at time t_{n+1}

$$\ddot{\mathbf{u}}_{n+1} = \frac{1}{\beta (\Delta t)^2}(\mathbf{u}_{n+1} - \mathbf{u}_n) - \frac{1}{\beta \Delta t}\dot{\mathbf{u}}_n + \left(1 - \frac{1}{2\beta} \right) \ddot{\mathbf{u}}_n \quad . \tag{35}$$

The accuracy and stability depends on the choice of the quadrature parameters $\beta \in]0,1]$ and $\gamma \in]0,1]$. For example, if $\beta = \frac{1}{4}$ and $\gamma = \frac{1}{2}$ (constant acceleration) or $\beta = \frac{1}{6}$ and $\gamma = \frac{1}{2}$ (linear acceleration), the Newmark method is unconditionally stable, i. e. its robustness is independent of Δt.

Hilber, Hughes, and Taylor (1978) extended Newmark's method by introducing the parameter α

$$\mathbf{M}\ddot{\mathbf{u}}\big|_{t_{n+1}} + (1+\alpha)(\mathbf{I}-\mathbf{P})\big|_{t_{n+1}} - \alpha(\mathbf{I}-\mathbf{P})\big|_{t_n} = \mathbf{0} \tag{36}$$

which shifts the force vector term from the new time point t_{n+1} to an intermediate time point $t_{n+1+\alpha}$ with $\alpha \in \left[-\frac{1}{3}, 0\right]$. This damps high frequencies and stabilizes the time integration scheme. A typical value is $\alpha = -\frac{1}{20}$. For $\alpha = 0$, the HHT algorithm is equivalent to Newmark's method.

- **The implicit Euler backward method**

Like the HHT method, the Euler backward method is an implicit time integration scheme, which implies that displacements

$$\mathbf{u}_{n+1} = \mathbf{u}_n + \Delta t\, \dot{\mathbf{u}}_{n+1} \tag{37}$$

and velocities

$$\dot{\mathbf{u}}_{n+1} = \dot{\mathbf{u}}_n + \Delta t\, \ddot{\mathbf{u}}_{n+1} \tag{38}$$

have to be updated iteratively. The Euler backward method is unconditionally stable.

When time increments become large, the dynamic response is affected by numerical damping, which is more distinct compared to the HHT method. Hence, the HHT integration scheme is a good choice, when dynamic effects are important, while the Euler backward method should be preferred over HHT for a quasi-static analysis.

- **The explicit midpoint method**

  No iterations are required for the explicit time integration scheme. Velocities

$$\dot{\mathbf{u}}_{n+1/2} = \dot{\mathbf{u}}_{n-1/2} + \frac{\Delta t_{n+1} + \Delta t_n}{2} \ddot{\mathbf{u}}_n \tag{39}$$

  and subsequently the displacements

$$\mathbf{u}_{n+1} = \mathbf{u}_n + \Delta t_{n+1} \dot{\mathbf{u}}_{n+1/2} \tag{40}$$

  are updated by means of the explicit midpoint rule. Multiplying the equation of motion, Eq. 31, with the inverse mass matrix $\mathbf{M}^{-1}$ yields the accelerations

$$\ddot{\mathbf{u}}_{n+1} = \mathbf{M}^{-1}(\mathbf{P}_{n+1} - \mathbf{I}_{n+1}) \tag{41}$$

  as a function of the internal forces $\mathbf{I}_{n+1} = \mathbf{I}(\mathbf{u}_{n+1}, \dot{\mathbf{u}}_{n+1/2})$ and the external forces $\mathbf{P}_{n+1} = \mathbf{P}(\mathbf{u}_{n+1}, \dot{\mathbf{u}}_{n+1/2})$. Since atoms are regarded as point masses, $\mathbf{M}$ is a diagonal mass matrix and thus can be easily inverted.

  The stability and accuracy depends on the time increment Δt. For linear problems, i. e. if the harmonic force field potentials are chosen, the optimal time increment size

$$\Delta t = \frac{2}{\omega_{\max}} \tag{42}$$

  is limited by the highest eigenfrequency $\omega_{\max}$. Since for systems including a large number of atoms, it is not feasible to determine $\omega_{\max}$, the highest element eigenfrequency or rather "bond eigenfrequency" $\omega_{\max}^{\text{elem}}$ can be used instead. In structural mechanics, this corresponds to a time increment size of

$$\Delta t = \frac{L_{\min}}{c} \tag{43}$$

where $L_{\min}$ is the smallest characteristic element dimension and c is the dilatational wave speed c of the material.

Based on the angular frequency $\omega = \sqrt{\frac{k}{m}}$ of the simple harmonic oscillator, we propose to update the time increment for each increment in accordance with Eq. 42

$$\Delta t = 2\eta \sqrt{\frac{m_{\mathrm{IJ}}}{|k_{\mathrm{IJ}}|}} \quad \text{with} \quad 0 < \eta \leq 1 \tag{44}$$

where k_{IJ} and m_{IJ} denote the current bond stiffness, which may also be negative, and the mass of the two atoms I and J. The parameter η controls accuracy and efficiency of the explicit time integration scheme, e. g. $\eta = 0.5$.

4.1.9 Relaxation step to determine the reference configuration

Usually, the equilibrium configuration of an atomic structure is unknown because the interatomic distances and angles differ from the natural bond distances and angles. From a numerical point of view, damping can help to determine the equilibrium state. The conformational analysis then becomes a "relaxation step". This technique can be compared to a conventional FEA analysis where initial stresses or bolt pretensions are applied in a first analysis step. In general, equilibrium configurations can be obtained in three different ways:

1. For statically determinate systems or symmetric structures such as graphene, it is possible to specify the coordinates of the atoms exactly.

2. If the structure is statically indeterminate, but the equilibrium configuration can be given approximately, a simple static analysis is sufficient. As an example, consider a (10,10) armchair carbon nanotube with a Stone-Wales defect. The initial configuration is shown in Fig. 5, top left. Using the nonlinear force field potentials, within a single static analysis step the equilibrium state shown top right can be reached. If more than one equilibrium configuration exists, a two-step static conformational analysis is recommended starting with the harmonic potentials.

3. For complex structures with multiple equilibrium states, convergence of a pure static analysis is quite unlikely. Even a dynamic analysis usually faces numerical problems because the initial potential energies of the bonds can be fairly high if the distance between two atoms is too close which often cannot be avoided. The high potential energy then is transformed to kinetic energy resulting in enormous oscillations or rather "explosions".

An example where numerical damping has to be introduced to dissipate the energy is elastomeric material. Fig. 5, bottom left, shows seven polymer chains which are interconnected by van der Waals forces. While the chemical bonds between the 107 atoms can be modeled in accordance with the natural lengths and angles, the van der Waals bonding lengths are generated more or less randomly. The equilibrium state shown bottom right is simulated using the Euler backward method in combination with an automatic time incrementation algorithm. Even though no additional damping is introduced, the quasi-static solution can be achieved in "only" about 250 time increments.

For static analyses and dynamic analyses using a different time integration scheme, it is recommended to start with large values for the damping parameters, e. g. for a Rayleigh damping model. During the relaxation step, damping should be reduced in accordance with the bonds' energies until a valid quasi-static equilibrium state is reached. The simulation times are comparable with the Euler backward scheme.

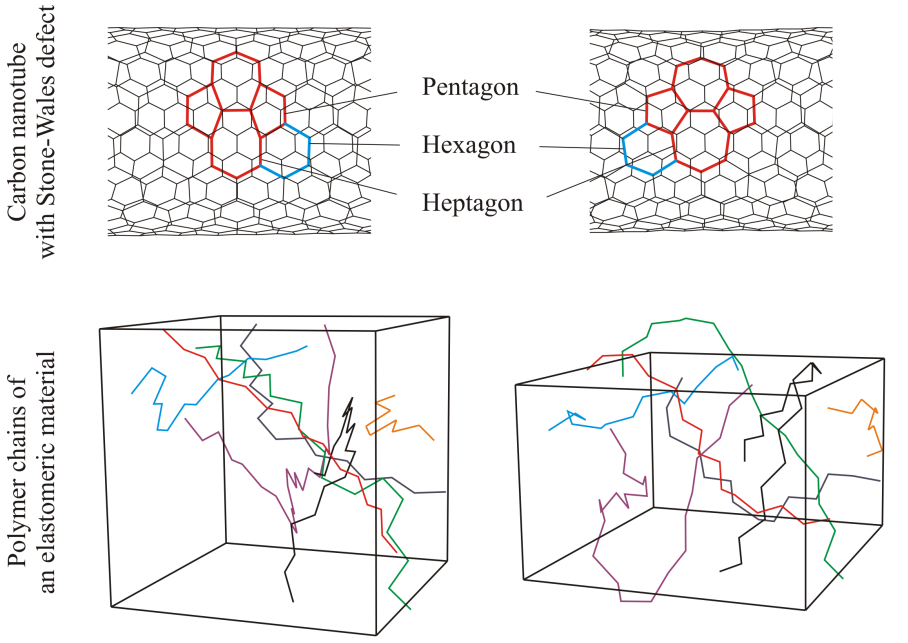

(a) Generated initial meshes (b) Equilibrium states after relaxation step

Figure 5: Reorganization of bonds during conformational analysis

4.2 User elements

Since conventional finite elements do not meet the requirements listed in the previous section, in the following, a new class of finite elements is introduced that can be used for MD simulations within the FEM framework. As pointed out in section 4.1.7, the developed finite elements which are presented in Fig. 6 only use translational degrees of freedom.

Bending and torsional moments are applied by means of force couples. The lever arms depend on the bond lengths R^0_{IJ}, R^0_{JK} and R^0_{KL} and angles Θ^0_J and Θ^0_K shown in Fig. 6(a). The force directions are described using the unit vectors depicted in Fig. 6(b). The 2-, 3- and 4-node elements for bond-stretch, bending and torsion given in Fig. 6(c), (d) and (e) have been implemented in the finite element codes Feap and Abaqus using a superposition technique.

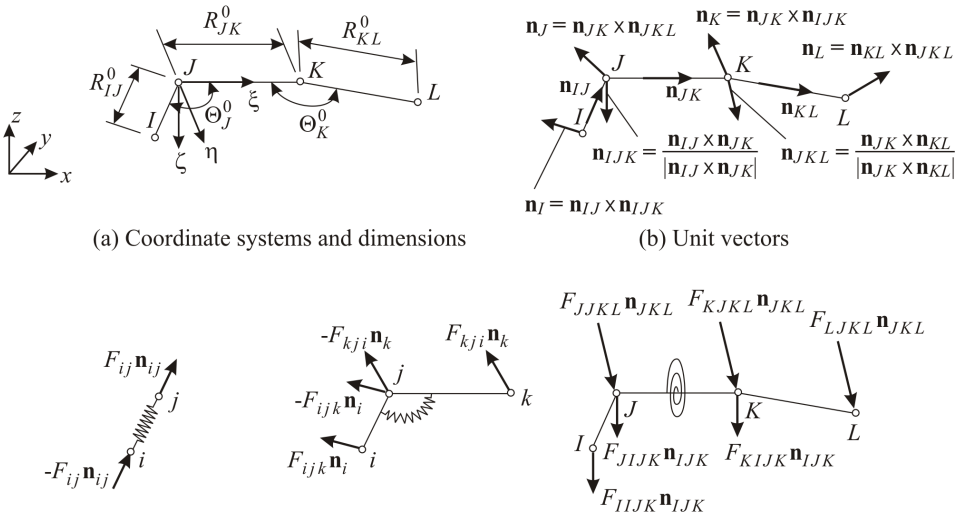

(a) Coordinate systems and dimensions (b) Unit vectors

(c) 2-node spring element (d) 3-node bending element (e) 4-node torsion element

Figure 6: Molecular dynamic finite elements without rotational degrees of freedom

In this section, the force vectors, the so-called right-hand-side vectors are given. They are obtained by derivatives of the force field potentials which respect to the atomic coordinates and have to be defined for all analysis types. In contrast to the explicit time integration scheme which does not use the Newton-Raphson method given in Appendix A, user elements for static and implicit dynamic analyses also require stiffness matrices. They can be found in Appendix B.

4.2.1 2-node element for bond stretch

The element force vector of the 2-node element includes the node vectors of the atoms i and j

$$\mathbf{F}_i = -F_{ij}\mathbf{n}_{ij} \quad , \quad \mathbf{F}_j = -\mathbf{F}_i \tag{45}$$

and can be used for both chemical and physical bonds. It is defined by its unit direction vector $\mathbf{n}_{ij}$ and the magnitude F_{ij} which depends on the force field potential. The derivative of Eq. 20 yields

$$F_{ij}^{\text{lin}} = k_{ij}(|\mathbf{x}_j - \mathbf{x}_i| - R_{ij}^0) \quad . \tag{46}$$

From the Morse potential Eq. 21 we get

$$\begin{aligned} F_{ij}^{\text{Morse}} = -2\alpha_{ij}n_{ij}D_{ij}\big[&\exp(-2\alpha_{ij}n_{ij}(|\mathbf{x}_j - \mathbf{x}_i| - R_{ij}^0)) \\ &- \exp(-\alpha_{ij}n_{ij}(|\mathbf{x}_j - \mathbf{x}_i| - R_{ij}^0))\big] \quad . \end{aligned} \tag{47}$$

For the Lennard-Jones (LJ) approach Eq. 23, the force magnitude is given as

$$F_{ij}^{\text{LJ}} = 12\frac{D_{ij,\text{vdW}}}{R_{ij,\text{vdW}}^0}\left[-\left(\frac{|\mathbf{x}_j - \mathbf{x}_i|}{R_{ij,\text{vdW}}^0}\right)^{-13} + \left(\frac{|\mathbf{x}_j - \mathbf{x}_i|}{R_{ij,\text{vdW}}^0}\right)^{-7}\right] \tag{48}$$

and the electrostatic force derived from Eq. 26 reads

$$F_{\text{Q}}(R_{IJ}) = -\frac{1}{4\pi\varepsilon_0}\frac{q_I q_J}{R_{IJ}^2} \quad . \tag{49}$$

Note that Coulomb forces can be neglected for the examples given in section 5.

4.2.2 3-node element for bending

The force vector of the 3-node bending element consists of the three components

$$\mathbf{F}_i = F_{ijk}\mathbf{n}_i \quad , \quad \mathbf{F}_k = F_{kji}\mathbf{n}_k \quad , \quad \mathbf{F}_j = -\mathbf{F}_i - \mathbf{F}_k \quad . \tag{50}$$

The magnitude F_{ijk} result from the derivative of the harmonic potential Eq. 27

$$F_{ijk}^{\text{lin}} = \frac{K_{ijk}}{R_{ij}^0}\left[\Theta_{ijk} - \Theta_j^0\right] \tag{51}$$

or the extended cosine approach Eq. 28

$$F_{ijk} = \begin{cases} -\dfrac{C_{ijk}}{R_{ij}^0}\left[\cos\Theta_{ijk} - \cos\Theta_j^0\right]\sin\Theta_{ijk} & \text{for} \quad \Theta_j^0 \neq 180^\circ \\ -\dfrac{K_{ijk}}{R_{ij}^0}\sin\Theta_{ijk} & \text{for} \quad \Theta_j^0 = 180^\circ \end{cases} \tag{52}$$

with respect to the unknown bending angle

$$\Theta_{ijk} = \arccos(-\mathbf{n}_{ij} \cdot \mathbf{n}_{jk}) \in [0^\circ, 180^\circ] \quad . \tag{53}$$

The unit vectors $\mathbf{n}_{ij}$ and $\mathbf{n}_{jk}$ defining Θ_{ijk} can be taken from Fig. 7. Considering that the lever arms are generally different, if follows for the magnitude

$$F_{kji} = F_{ijk} \frac{R^0_{ij}}{R^0_{jk}} \quad . \tag{54}$$

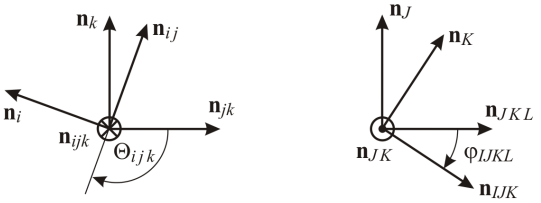

Figure 7: Bending and torsion angles derived from unit vectors

At this point it should be noted that angles between 180° and 360° can be omitted. For symmetry reasons, they are covered by the torsion potential with its 0°- and 180°-equilibrium angles. For example, the combination $\Theta_{ijk} = 190^\circ$ and $\varphi_{IJKL} = 4^\circ$ is equivalent to $\Theta_{ijk} = 170^\circ$ and $\varphi_{IJKL} = 184^\circ$.

Instead of Eq. 53 for the computation of the bending angle, many authors suggest to make use of the formula $\Theta_{ijk} = 180^\circ - \arcsin|\mathbf{n}_{ij} \times \mathbf{n}_{jk}|$. However, it is necessary to point out that this approach is not suitable for large deformations because it only covers values between 90° and 180°.

4.2.3 4-node element for torsion

As shown in Fig. 6(e), there are six concentrated forces acting on the 4-node torsion element whose magnitudes generally differ from each other. The element vector

$$\begin{aligned}
\mathbf{F}_I &= F_{IIJK}\mathbf{n}_{IJK} \\
\mathbf{F}_L &= F_{LJKL}\mathbf{n}_{JKL} \\
\mathbf{F}_J &= F_{JIJK}\mathbf{n}_{IJK} + F_{JJKL}\mathbf{n}_{JKL} &&= \alpha_{JIJK}\mathbf{F}_I + \frac{\alpha_{JJKL}}{\alpha_{LJKL}}\mathbf{F}_L \\
\mathbf{F}_K &= F_{KIJK}\mathbf{n}_{IJK} + F_{KJKL}\mathbf{n}_{JKL} &&= \alpha_{KIJK}\mathbf{F}_I + \frac{\alpha_{KJKL}}{\alpha_{LJKL}}\mathbf{F}_L
\end{aligned} \tag{55}$$

contains four node vectors. While the first index of the force magnitudes denotes the node the force is acting on, indices 2 to 4 refer to one of the two planes IJK and JKL, represented by the unit vectors $\mathbf{n}_{IJK}$ and $\mathbf{n}_{JKL}$, see Fig. 7.

Considering the lever arm $R^0_{IJ}\sin\Theta^0_J$, the magnitude F_{IIJK} follows from the derivative of Eq. 30

$$F^{\text{lin}}_{IIJK} = -\frac{V_{IJKL}\,n^2_{JK}}{2R^0_{IJ}\sin\Theta^0_J}\,(\varphi_{IJKL}-\varphi^0_{JK}) \tag{56}$$

or Eq. 29

$$F_{IIJK} = -\frac{V_{IJKL}\,n_{JK}}{2R^0_{IJ}\sin\Theta^0_J}\,\sin\left[n_{JK}(\varphi_{IJKL}-\varphi^0_{JK})\right] \tag{57}$$

with respect to the dihedral angle φ_{IJKL}. For the determination of φ_{IJKL}, a case distinction is required depending on the number of natural angles φ^0_{JK}, e. g. for graphene $\varphi^0_{JK}=0^\circ$ if $\mathbf{n}_{IJK}\cdot\mathbf{n}_{JKL}\geq 0$ or $\varphi^0_{JK}=180^\circ$ if $\mathbf{n}_{IJK}\cdot\mathbf{n}_{JKL}<0$, and thus:

$$\varphi_{IJKL} = \begin{cases} +\arcsin[(\mathbf{n}_{IJK}\times\mathbf{n}_{JKL})\cdot\mathbf{n}_{JK}]\in[-90^\circ,+90^\circ] & \text{for } \mathbf{n}_{IJK}\cdot\mathbf{n}_{JKL}\geq 0 \\ 180^\circ-\arcsin[(\mathbf{n}_{IJK}\times\mathbf{n}_{JKL})\cdot\mathbf{n}_{JK}]\in[+90^\circ,+270^\circ] & \text{for } \mathbf{n}_{IJK}\cdot\mathbf{n}_{JKL}<0\,. \end{cases} \tag{58}$$

Furthermore, it is necessary to project the cross product $\mathbf{n}_{IJK}\times\mathbf{n}_{JKL}$ on the associated unit vector $\mathbf{n}_{JK}$ in order to determine the sign of φ_{IJKL} for $\varphi^0_{JK}=0^\circ$ or rather if φ_{IJKL} is larger or smaller than 180° for $\varphi^0_{JK}=180^\circ$.

From simple geometric considerations, we get the magnitudes

$$F_{KIJK}\underbrace{-\frac{R^0_{IJ}\cos\Theta^0_J}{R^0_{JK}}}_{=\alpha_{KIJK}}F_{IIJK} \quad , \quad F_{JIJK} = -F_{IIJK}-F_{KIJK} = \underbrace{(-1-\alpha_{KIJK})}_{=\alpha_{JIJK}}F_{IIJK} \tag{59}$$

associated with plane IJK and the forces

$$\begin{aligned} F_{LJKL} &= \underbrace{-\frac{R^0_{IJ}\sin\Theta^0_J}{R^0_{KL}\sin\Theta^0_K}}_{=\alpha_{LJKL}}F_{IIJK} \\ F_{JJKL} = -\frac{R^0_{KL}\cos\Theta^0_K}{R^0_{JK}}F_{LJKL} \quad &= \underbrace{(-\alpha_{LJKL}\frac{R^0_{KL}\cos\Theta^0_K}{R^0_{JK}})}_{=\alpha_{JJKL}}F_{IIJK} \\ F_{KJKL} = -F_{LJKL}-F_{JJKL} \quad &= \underbrace{(-\alpha_{LJKL}-\alpha_{JJKL})}_{=\alpha_{KJKL}}F_{IIJK} \end{aligned} \tag{60}$$

which act normal to plane JKL.

To avoid a coupling of the different energy potentials, changes of the lever arms due to changes of the equilibrium distances are neglected.

4.3 Inversion

Some force fields such as the Dreiding approach also include potential energies for inversion. In geometry, inversion in a point or point reflection is equivalent to a 180°-rotation and a reflection at a plane, as illustrated in Fig. 8. In molecular dynamics, inversion is only relevant when at least four atoms are involved which must be arranged in a specific manner. In contrast to torsion, where the four atoms form a chain-like structure, three atoms form a triangle through which the fourth may pass. Hence, for some structures such as elastomeric material consisting of several polymer chains, inversion is irrelevant.

It is not trivial to set up an appropriate potential since inversion can be separated from the other energy forms only in very rare cases such as for ammonia NH_3. For most molecules, interactions between inversion and torsion energy and, for spacial structures, also bending energy has to be considered. Therefore, some approaches such as the CHARMM force field represent inversion by "improper" torsion, i. e. inversion is incorporated by means of torsion energy.

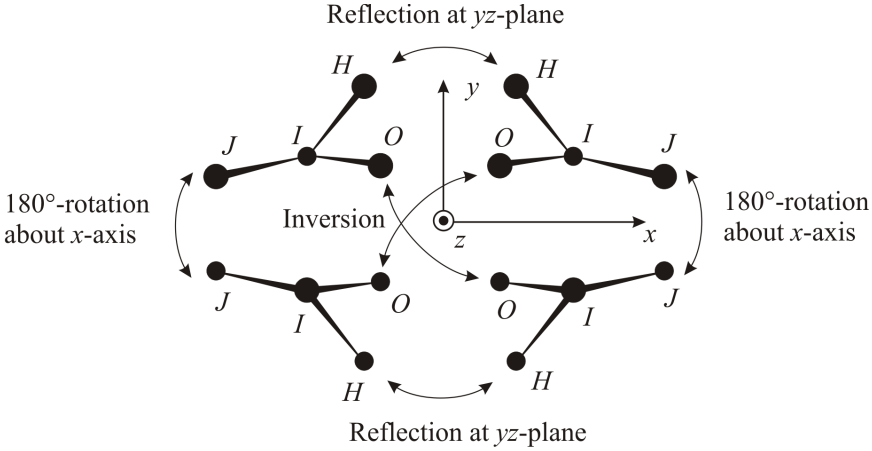

Figure 8: Inversion as a combination of rotation and reflection

4.3.1 Spacial structures

From a mechanical point of view, inversion of spacial structures such as an ammonia molecule NH_3 is a snap-through problem, as illustrated in Fig. 9. As opposed to planar structures, spatial structures have two equilibrium states or even more if multiple local inversions can occur. Ammonia has two natural bending angles: $\Theta_J^0 = 106.7^\circ$ and $2 \cdot 120^\circ - 106.7^\circ = 133.3^\circ$.

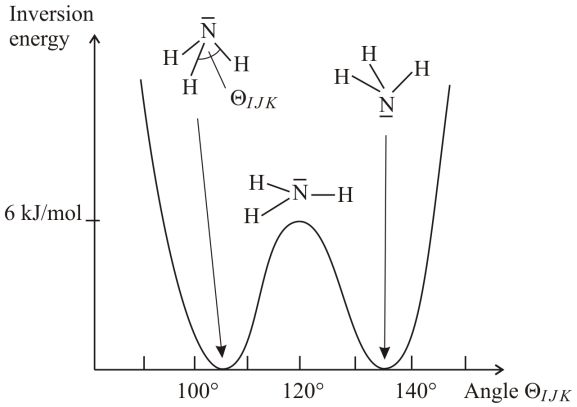

Figure 9: Energy profile during snap-through (inversion) of a NH_3-molecule

4.3.2 Planar structures

For planar structures such as graphene, inversion refers to the motion of an atom out of the plane defined by its three neighbors, cf. Fig. 10(a). The out-of-plane displacement w of node I is expressed by the inversion angle

$$\Psi = \Psi_\mathrm{l} + \Psi_\mathrm{r} = \arctan\left(\frac{2w}{R_\mathrm{e}}\right) + \arctan\left(\frac{w}{R_\mathrm{e}}\right) \tag{61}$$

which corresponds to the angle between plane HIO and bond IJ. Due to the structure's symmetry, the same angle can be found between plane IJO and bond HI and between plane IJH and bond IO. As depicted in Fig. 10(b), the deformation leads to so-called "improper" torsion, e. g. for the atoms I, J, K and L.

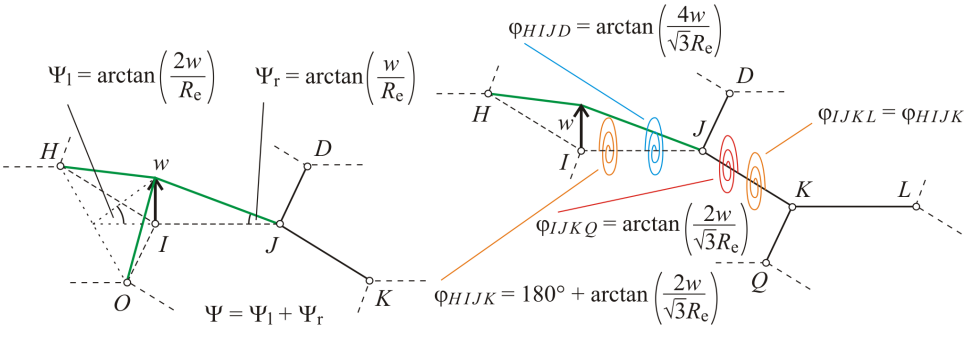

(a) Inversion (b) Additional torsion

Figure 10: Improper torsion resulting from inversion for the example of graphene

Fig. 11 illustrates that a total of 24 torsion angles are affected when atom I is moved out of plane HJO. For small deformations, the following torsion angles emerge:

$$\begin{aligned}
&\varphi_{HIJD} = \varphi_{OIHG} = \varphi_{JIOP} = +\frac{4w}{\sqrt{3}R_e} \quad , \quad \varphi_{OIJK} = \varphi_{JIHB} = \varphi_{HION} = -\frac{4w}{\sqrt{3}R_e} \\
&\varphi_{IJKQ} = \varphi_{IHBC} = \varphi_{IONM} = +\frac{2w}{\sqrt{3}R_e} \quad , \quad \varphi_{IJDC} = \varphi_{IHGM} = \varphi_{IOPQ} = -\frac{2w}{\sqrt{3}R_e} \\
&\varphi_{HIJK} = \varphi_{OIHB} = \varphi_{JION} = \varphi_{IJKL} = \varphi_{IHBA} = \varphi_{IONS} = 180^\circ + \frac{2w}{\sqrt{3}R_e} \\
&\varphi_{OIJD} = \varphi_{JIHG} = \varphi_{HIOP} = \varphi_{IJDE} = \varphi_{IHGF} = \varphi_{IOPT} = 180^\circ - \frac{2w}{\sqrt{3}R_e} \quad .
\end{aligned} \tag{62}$$

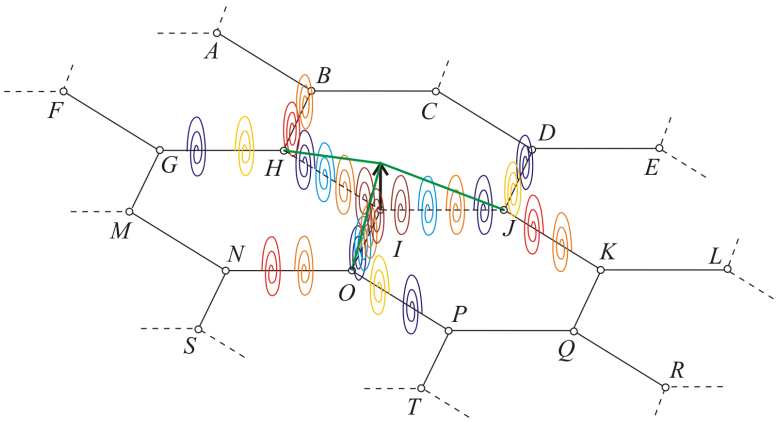

Figure 11: Torsion angles affected by deflection of atom I out of plane defined by atoms H, J and O with color coding according to Eq. 62

4.3.3 Force field potentials

In spectroscopy, the calculation of the inversion energy is often carried out with the help of the linear approach

$$E_I^{\text{lin}} = \frac{1}{2} K_{\text{inv}} (\Psi - \Psi_0)^2 \quad . \tag{63}$$

To address the fact that the derivative of the inversion energy has to vanish, $\frac{dE_I}{d\Psi} = 0$, when reaching the snap-through point $\Psi = 0^\circ$, Mayo, Olafson, and Goddard (III)

(1990) suggest the following formulation:

$$E_{\mathrm{I}} = \begin{cases} \frac{1}{2} C_{\mathrm{inv}} (\cos\Psi - \cos\Psi_0)^2 & \text{for} \quad \Psi_0 \neq 0^\circ \\ K_{\mathrm{inv}} (1 - \cos\Psi) & \text{for} \quad \Psi_0 = 0^\circ \end{cases} \tag{64}$$

with the stiffness $K_{\mathrm{inv}} = \sin^2\Psi_0 C_{\mathrm{inv}}$, e. g. $K_{\mathrm{inv}} = 40 \frac{\mathrm{kcal}}{\mathrm{mol\,rad}^2}$ for graphene. The approach distinguishes between spatial structures $\Psi_0 \neq 0^\circ$ and planar structures $\Psi_0 = 0^\circ$. For spatial structures, the maximum energy at the snap-through point $\Psi = 0^\circ$ is

$$E_{\mathrm{I}}^{\mathrm{bar}} = 2 C_{\mathrm{inv}} \sin^2 \left(\frac{1}{2} \Psi_0 \right) \quad , \tag{65}$$

e. g. $E_{\mathrm{I}}^{\mathrm{bar}} = 6 \frac{\mathrm{kcal}}{\mathrm{mol}}$ for ammonia.

4.3.4 Modeling inversion by improper torsion

For planar structures, the inversion energy can be taken into account using additional torsion energy. For demonstration purposes, we consider the example of graphene shown in Fig. 10 and Fig. 11. The deflection w of atom I leads to an inversion energy with the direct neighbors H, J and O. As a consequence, atom J moves out of its plane IDK by $-\frac{w}{3}$, etc.

With the inversion and torsion angles given in Eq. 61 and Eq. 62, the ratio of inversion energy to torsion energy for small deformations can be derived as:

$$\begin{aligned} \frac{E_{\mathrm{I,ges}}^{\mathrm{lin}}}{E_{\mathrm{T,ges}}^{\mathrm{lin}}} &= \frac{E_{\mathrm{I}}^{\mathrm{lin}}(\Psi_{\mathrm{l}} + \Psi_{\mathrm{r}}) + 3 E_{\mathrm{I}}^{\mathrm{lin}}(\Psi_{\mathrm{r}})}{6 E_{\mathrm{T}}^{\mathrm{lin}}(\varphi_{HIJD}) + 18 E_{\mathrm{T}}^{\mathrm{lin}}(\varphi_{IJKQ})} = \\ &= \frac{\frac{1}{2} K_{\mathrm{inv}} \left(\frac{3w}{R_{\mathrm{e}}} \right)^2 + 3 \cdot \frac{1}{2} K_{\mathrm{inv}} \left(\frac{w}{R_{\mathrm{e}}} \right)^2}{6 \cdot \frac{1}{4} V_{IJKL} n_{JK}^2 \left(\frac{4w}{\sqrt{3} R_{\mathrm{e}}} \right)^2 + 18 \cdot \frac{1}{4} V_{IJKL} n_{JK}^2 \left(\frac{2w}{\sqrt{3} R_{\mathrm{e}}} \right)^2} = \\ &= \frac{6 K_{\mathrm{inv}}}{14 V_{IJKL} n_{JK}^2} = \frac{6 \cdot 40}{14 \cdot 6.25 \cdot 2^2} = 68.6\,\% \quad . \end{aligned} \tag{66}$$

Hence, torsional stiffness has to be increased by 68.6 % while, in turn, the inversion energy can be neglected. This way, we can obtain identical results for planar symmetric structures like graphene if deformations are small. For large deformations, a small error has to be accepted. Nevertheless, this approach is recommended as it is favorable from a mathematical and mechanical point of view when all energy forms are independent of one another.

5 Numerical Examples

In order to demonstrate the capabilities of MDFEM and to verify the robustness and reliability of the finite elements introduced in section 4.2, two different examples are presented. The first one deals with single-walled carbon nanotubes as for such structures chemical bonds are dominant. Neglecting physical interactions, even with an implicit time integration scheme, structures with more than 1 million atoms can be simulated.

For the second example, a model of elastomeric material, physical bondings have to be considered. As a consequence, static and implicit dynamic analyses are limited to a few thousand atoms because the long-range potentials lead to a very large bandwidth of the stiffness matrix. To overcome this limitation, the explicit midpoint method is used.

5.1 Torsion of single-walled carbon nanotube

Carbon nanotubes are subject of many numerical investigations in literature, as their mechanical and electrical properties are remarkable, but very hard to determine experimentally. Defects e. g. stemming from the manufacturing process may lead to drastic changes in the material behavior.

A systematic investigation of the effects of atomistic defects on the nanomechanical properties and fracture behavior of single-walled carbon nanotubes using MD simulation is e. g. provided by Cheng, Hsu, and Chen (2009). Their results show that the properties highly depend on the defect rate but also on the distribution pattern and that the failure of the nanotubes can be regarded as brittle whereas the cracks propagate along the areas with high tensile stress concentration.

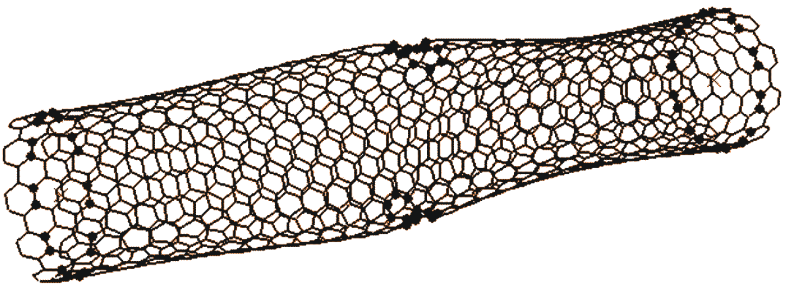

Figure 12: Buckling of carbon nanotube with two Stone-Wales defects at the top and at the bottom (SW3) at about 50°-torsion

The effects of the nanotube helicity, the nanotube diameter and the percentage of vacancy defects on the bond length, bond angle and tensile strength of zigzag and armchair single-walled carbon nanotubes is subject of a study by Jeng, Tsai, Huang, and Chang (2009). A good agreement of the stress-strain response between molecular dynamics and molecular statics simulations is observed.

The MDFEM simulation in Fig. 12 shows the failure mode of a (10,10)-armchair carbon nanotube with two Stone-Wales defects at a torsion angle of about 50°. The cross-section, which is initially circular adopts an elliptic shape that propagates helically over the entire length of the tube until the opposite walls come close to each other. A similar behavior was observed by Rochefort, Avouris, Lesage, and Salahub (1999) and Chakrabarty and Cagin (2008).

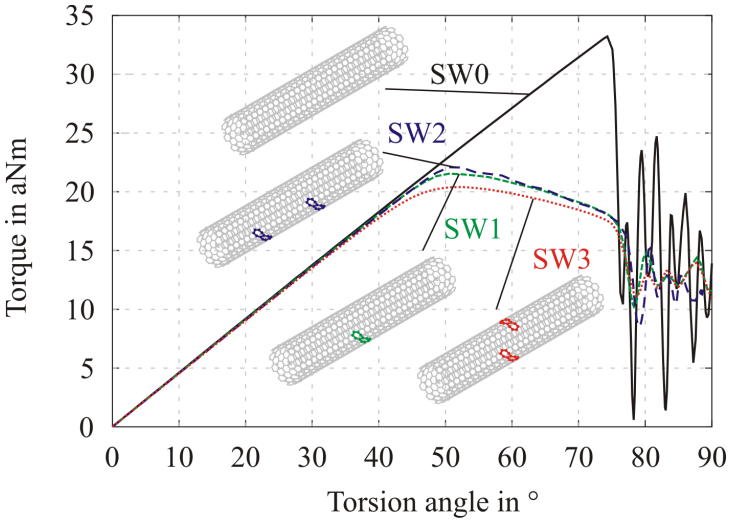

Figure 13: Influence of Stone-Wales defects on torsion load resistance

The torque-rotation curves in Fig. 13 demonstrate the influence of the Stone-Wales (SW) defects. While for a nanotube without defects (SW0) a bifurcation can be observed, defects transform the bifurcation problem into a snap-through problem. Instead of an instantaneous collapse the shape of the nanotube changes slowly. The maximum torsional moment of 33 aNm (SW0) decreases to 22 aNm for the nanotube with two defects at the bottom site (SW2), 21.5 aNm for the nanotube with only one defect (SW1) and 20 aNm for the nanotube in Fig. 12 with two opposing defects (SW3).

At this point, it should be stressed that the results are identical to a classical MD simulation, given that the same force field potentials are applied. Here, we used

the Dreiding approach proposed by Mayo, Olafson, and Goddard (III) (1990). The reader who is interested in different load cases, namely when the nanotubes are subjected to tension, compression or bending loads, is referred to the publication by Nasdala, Ernst, Lengnick, and Rothert (2005).

5.2 Inelastic behavior of elastomeric material

As pointed out in section 4.1.9, MDFEM simulations usually start with a relaxation step. Elastomeric material is a good example where it is impossible to guess a valid equilibrium state. In addition to the challenging conformational analysis, this example also provides explanations for inelastic material behavior. Using elastic force field potentials, it is possible to simulate softening and hysteresis effects.

5.2.1 Relaxation step

For demonstration purposes, we start with the small example shown in Fig. 5, bottom. Since only 107 atoms are involved, it is possible to apply the implicit Euler backward method for the relaxation step. This method is very efficient since large time increments lead to high numerical damping which dissipates the kinetic energy of the system.

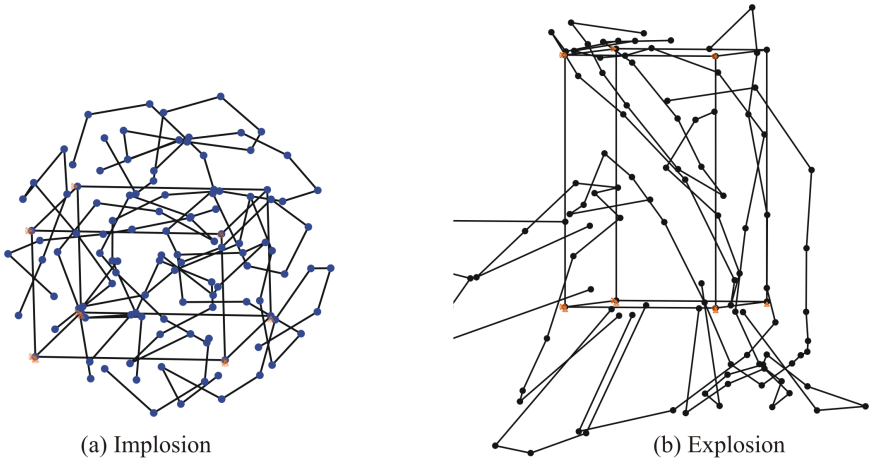

(a) Implosion (b) Explosion

Figure 14: Convergence problems of analyses without damping

If the implicit HHT method is used without introducing additional damping, the analysis does not converge, as demonstrated in Fig. 14. In contrast to the equilibrium state, the van der Waals bond energies are significantly higher than the bond stretch energies of the chemical bonds. This stems from the fact that the van der

Waals bond energies are very high for atoms close to each other according to the Lennard-Jones approach. In a dynamic analysis, the potential energy is transformed to kinetic energy but as the bond fracture energies are small compared to the initial bond potential energies, the bonds are destroyed. Depending on the size of the RVE, an "implosion" may occur first, then followed by an "explosion" or, if the RVE is small, the analysis already starts with the second part.

For larger structures, which may be more than 1000 atoms, the explicit time integration method is preferable. For the example shown in Fig. 15 that consists of 10051 atoms, computational costs can be efficiently reduced, when the analysis starts with a very high amount of damping, e. g. α-Rayleigh damping, which then is reduced in about 10 steps, each time by an order of magnitude. This approach can be optimized by setting the velocities to zero before starting each new step.

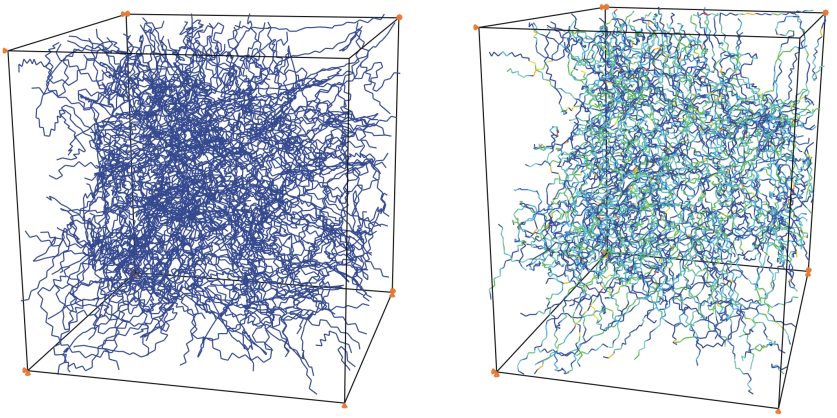

(a) Generated initial mesh (b) Equilibrium state after relaxation step

Figure 15: Conformational analysis of an elastomer with 10051 atoms

5.2.2 Loading step

Both models are subjected to cyclic loading at 25 %, 50 % and 100 % strain amplitude, 3 cycles at each amplitude. Constraints keep the volume of the RVE constant. The loading can be regarded as quasi-static. As can be seen in Fig. 16 for cycles 4 to 6 of the 107-atom model, there is a continuous rearrangement of chains within the polymer network. The chemical bonds can sustain the applied load. Some van der Waals interactions, however, break when the fracture energy is exceeded while other interactions come into existence when two atoms approach each other. Note that the physical bondings as well as covalent interchain cross-linkages, build during the vulcanization process, are not shown, for the sake of clarity.

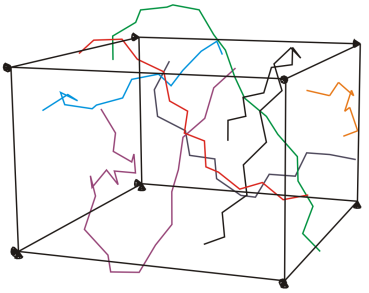

(a) 0% strain (initial equilibrium state)

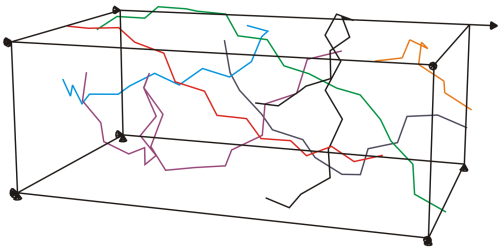

(b) 50% strain (4. cycle)

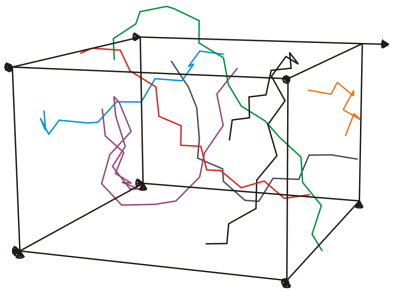

(c) 0% strain (start of 5. cycle)

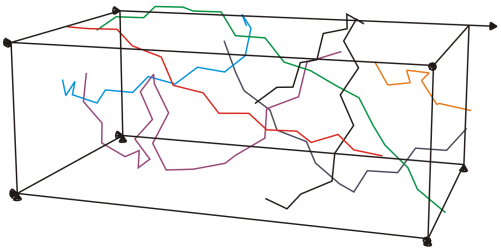

(d) 50% strain (5. cycle)

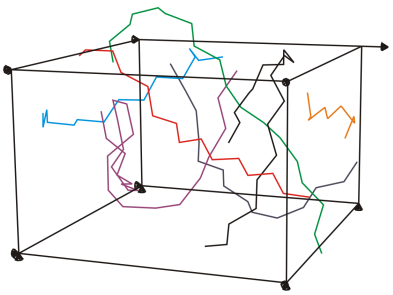

(e) 0% strain (start of 6. cycle)

(f) 50% strain (6. cycle)

Figure 16: Continuous reorganization of bonds during cyclic loading

The 107-atom model is too small for being representative, i. e. the load-deflection curve is very jagged and similar models would lead to different results. Therefore, we shall discuss only the response of the 10051-atom model, shown in Fig. 17.

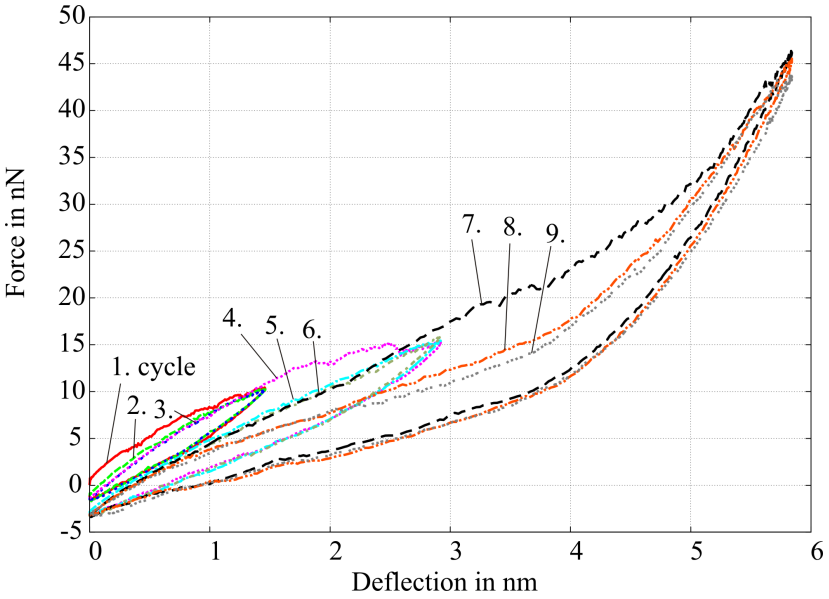

Figure 17: Load-deflection curve of an elastomer with 10051 atoms

It is remarkable that all the main characteristics of elastomeric materials, namely

- the Mullins effect (softening),
- curvature change from negative to positive,
- a permanent set (plasticity or viscoelasticity), and
- hysteresis loops (energy dissipation)

can be found in the simulated force-deflection curve though only (elastic) force fields potentials are used.

It should be noted that the load-deflection curve is not smooth. This is due to the fact that a rupture of bondings reduces the overall stiffness while the creation of bondings strengthens the structure.

The results proof that it is generally possible to simulate inelastic material behavior without using damping or friction elements. The underlying mechanism is the rearrangement of bondings which causes the polymer chains to vibrate. Potential energy is transformed to kinetic energy. The oscillations on the nanoscale can be observed on the macroscale as a temperature increase of the material.

6 Conclusions

It is possible to perform molecular dynamic simulations within the framework of the finite element method. However, this is not an easy task since a special class of finite elements are required for force fields using multi-body potentials. This paper presents the theoretical background of the MDFEM elements as well as guidelines for the implementation and usage.

Apart from mesh generation techniques, which are not covered, all important aspects of MDFEM are discussed from a FEA software user's point of view: what time integration schemes are usually available and when to use which, what is the difference between natural and equilibrium bond lengths and angles, how to obtain an equilibrium configuration, or when inversion energy is important and how it can be transformed to torsion energy. Two examples demonstrate the accuracy and efficiency of the introduced MDFEM elements.

MDFEM provides a framework that is more than performing simple MD simulations. Conventionally, MD programs are used in chemistry and physics to perform conformational studies based on force fields. Goal is to determine equilibrium states rather than to study the response of atomic structures under mechanical loading.

The main benefit of MDFEM is that concurrent multiscale simulations, i. e. a combination of continuum and atomistic regions, are feasible. Complex models can be developed to predict e. g. the properties of composites containing nanoparticles which determine the macroscopic material behavior. For such models, parametric studies in terms of computer-aided material design can be carried out to analyze the influence of changes in the atomic structure, namely the particle size, distribution or the particle-matrix interface. The results can then be used to identify the basic mechanisms that lead to the enhancement of characteristic values of such composites and subsequently exploited to improve the manufacturing processes.

Acknowledgement: The authors acknowledge funding by the Helmholtz Association of German Research Centres. The Institute of Structural Analysis (ISD) is member of its virtual institute "Nanotechnology in Polymer Composites". ISD is also member of the Laboratory of Nano and Quantum Engineering (LNQE), the support of which is gratefully acknowledged.

References

Allinger, N. L.; Chen, K. (1996): Hyperconjugative effects on carbon-carbon bond lengths in molecular mechanics (MM4). *Journal of Computational Chemistry*, vol. 17, pp. 747–755.

Arroyo, M.; Belytschko, T. (2002): An atomistic-based finite deformation membrane for single layer crystalline films. *Journal of the Mechanics and Physics of Solids*, vol. 50, no. 9, pp. 1941–1977.

Bloch, F. (1928): Über die Quantenmechanik der Elektronen in Kristallgittern. *Zeitschrift für Physik*, vol. 52, pp. 555–600.

Born, M.; Huang, K. (1954): *Dynamical theory of crystal lattices*. Oxford University Press, Oxford.

Brenner, D. W. (1990): Empirical potential for hydrocarbons for use in simulating the chemical vapor deposition of diamond films. *Physical Review B*, vol. 42, no. 15, pp. 9458–9471.

Brooks, B. R.; Bruccoleri, R. E.; Olafson, B. D.; States, D. J.; Swaminathan, S.; Karplus, M. (1983): CHARMM: A program for macromolecular energy, minimization, and dynamics calculations. *Journal of Computational Chemistry*, vol. 4, pp. 187–217.

Buckingham, R. A. (1938): The classical equation of state of gaseous helium, neon and argon. *Proceedings of the Royal Society of London. Series A, Mathematical and Physical Sciences*, vol. 168, no. 933, pp. 264–283.

Car, R.; Parrinello, M. (1985): Unified approach for molecular dynamics and density functional theory. *Physical Review Letters*, vol. 55, no. 22, pp. 2471–2474.

Chakrabarty, A.; Cagin, T. (2008): Computational studies on mechanical and thermal properties of carbon nanotube based nanostructures. *CMC: Computers, Materials & Continua*, vol. 7, no. 3, pp. 167–189.

Cheng, H.-C.; Hsu, Y.-C.; Chen, W.-H. (2009): The influence of structural defect on mechanical properties and fracture behaviors of carbon nanotubes. *CMC: Computers, Materials & Continua*, vol. 11, no. 2, pp. 127–146.

Dirac, P. (1930): Note on exchange phenomena in the Thomas atom. *Proceedings of the Cambridge Philosophical Society*, vol. 26, pp. 376–385.

Ehrenfest, P. (1927): Bemerkung über die angenäherte Gültigkeit der klassischen Mechanik innerhalb der Quantenmechanik. *Zeitschrift für Physik*, vol. 45, pp. 455–457.

Ercolessi, F.; Adams, J. (1994): Interatomic potentials from first-principles calculations: The force-matching method. *Europhysics Letters*, vol. 26, pp. 583–588.

Ericksen, J. L. (1984): The cauchy and born hypotheses for crystals. In Gurtin, M. E.(Ed): *Phase Transformations and Material Instabilities in Solids*, pp. 61–77. Academic Press, Inc., New York.

Fock, V. (1930): Näherungsmethode zur Lösung des quantenmechanischen Mehrkörperproblems. *Zeitschrift für Physik*, vol. 61, pp. 126–148.

Harik, V. M. (2002): Mechanics of carbon nanotubes: applicability of the continuum-beam models. *Computational Materials Science*, vol. 24, pp. 328–342.

Hartree, D. R. (1928): The wave mechanics of an atom with a noncoulomb central field. Part I: theory and methods. *Proceedings of the Cambridge Philosophical Society*, vol. 24, pp. 89.

Hartree, D. R. (1932): A practical method for the numerical solution of differential equations. *Memoirs and Proceedings of the Manchester Literary & Philosophical Society*, vol. 77, pp. 91.

Hilber, H. M.; Hughes, T. J. R.; Taylor, R. L. (1978): Collocation, dissipation and 'overshoot' for time integration schemes in structural dynamics. *Earthquake Engineering and Structural Dynamics*, vol. 6, pp. 99–117.

Hohenberg, P.; Kohn, W. (1964): Inhomogeneous electron gas. *Physical Review*, vol. 136, no. 3B, pp. 864–871.

Jeng, Y.-R.; Tsai, P.-C.; Huang, G.-Z.; Chang, I.-L. (2009): An investigation into the mechanical behavior of single-walled carbon nanotubes under uniaxial tension using molecular statics and molecular dynamics simulations. *CMC: Computers, Materials & Continua*, vol. 11, no. 2, pp. 109–125.

Kohn, W.; Sham, J. (1965): Self-consistent equations including exchange and correlation effects. *Physical Review*, vol. 140, no. 4A, pp. 1133–1138.

Lennard-Jones, J. E. (1929): The electronic structure of some diatomic molecules. *Transactions of the Faraday Society*, vol. 25, pp. 668–686.

Levine, I. N. (1991): *Quantum Chemistry*. Prentice-Hall, New York, 4 edition.

Li, C.; Chou, T.-W. (2004): Modeling of elastic buckling of carbon nanotubes by molecular structural mechanics approach. *Mechanics of Materials*, vol. 36, no. 11, pp. 1047–1055.

Marx, D.; Hutter, J. (2000): Ab initio molecular dynamics: Theory and implementation. In Grotendorst, J.(Ed): *Modern Methods and Algorithms of Quantum Chemistry*, pp. 301–449. John von Neumann Institute for Computing, Jülich.

Mayo, S. L.; Olafson, B. D.; Goddard (III), W. A. (1990): DREIDING: A generic force field for molecular simulations. *Journal of Physical Chemistry*, vol. 94, pp. 8897–8909.

Morse, P. M. (1929): Diatomic molecules according to the wave mechanics II: Vibrational levels. *Physical Review*, vol. 34, pp. 57–64.

Nasdala, L.; Ernst, G. (2005): Development of a 4-node finite element for the computation of nano-structured materials. *Computational Materials Science*, vol. 33, no. 4, pp. 443–458.

Nasdala, L.; Ernst, G.; Lengnick, M.; Rothert, H. (2005): Finite element analysis of carbon nanotubes with Stone-Wales defects. *CMES: Computer Modeling in Engineering & Sciences*, vol. 7, no. 3, pp. 293–304.

Newmark, N. M. (1959): A method of computation for structural dynamics. *Journal of Engineering Mechanics Division*, vol. 85, pp. 67–94.

Pauling, L.; Wilson Jr., E. B. (1985): *Introduction to Quantum Mechanics with Applications to Chemistry*. Dover, New York.

Rappé, A. K.; Casewit, C. J.; Colwell, K. S.; Goddard (III), W. A.; Skiff, W. M. (1992): UFF, a full periodic table force field for molecular mechanics and molecular dynamics simulations. *Journal of the American Chemical Society*, vol. 114, pp. 10024–10035.

Rochefort, A.; Avouris, P.; Lesage, F.; Salahub, D. R. (1999): Electrical and mechanical properties of distorted carbon nanotubes. *Physical Review B*, vol. 60, no. 19, pp. 13824–13830.

Roterman, I. K.; Lambert, M. H.; Gibson, K. D.; Scheraga, H. A. (1989): A comparison of the CHARMM, AMBER and ECEPP potentials for peptides. I. Conformational predictions for the tandemly repeated peptide $(\text{Asn-Ala-Asn-Pro})_9$. *Journal of Biomolecular Structures and Dynamics*, vol. 7, pp. 391–419.

Schlick, T. (2002): *Molecular Modeling and Simulation*. Springer, New York.

Schrödinger, E. (1926): Quantisierung als Eigenwertproblem. *Annalen der Physik*, vol. 79, pp. 361–376, 489–527.

Shen, S.; Atluri, S. N. (2004): Computational nano-mechanics and multi-scale simulation. *CMC: Computers, Materials & Continua*, vol. 1, no. 1, pp. 59–90.

Slater, J. C.; Koster, G. F. (1954): Simplified LCAO method for the periodic potential problem. *Physical Review*, vol. 94, no. 6, pp. 1498–1524.

Slater, J. C.; Wilson, T. M.; Wood, J. H. (1969): Comparison of several exchange potentials for electrons in the Cu+ ion. *Physical Review*, vol. 179, no. 1, pp. 28–38.

Stillinger, F. H.; Weber, T. A. (1985): Computer simulation of local order in condensed phases of silicon. *Physical Review B*, vol. 31, no. 8, pp. 5262–5271.

Tersoff, J. (1988): Empirical interatomic potential for carbon, with applications to amorphous carbon. *Physical Review Letters*, vol. 61, no. 25, pp. 2879–2882.

Tserpes, K. I.; Papanikos, P. (2005): Finite element modeling of single-walled carbon nanotubes. *Composites Part B: Engineering*, vol. 36, pp. 468–477.

van Duin, A. C. T.; Dasgupta, S.; Lorant, F.; Goddard (III), W. A. (2001): Reaxff: A reactive force field for hydrocarbons. *The Journal of Physical Chemistry A*, vol. 105, no. 41, pp. 9396–9409.

Verlet, L. (1967): Computer experiments on classical fluids. I. Thermodynamical properties of Lennard-Jones molecules. *Physical Review*, vol. 159, no. 1, pp. 98.

Wang, X. Y.; Wang, X. (2004): Numerical simulation for bending modulus of carbon and some explanations for experiment. *Composites Part B: Engineering*, vol. 35, pp. 79–86.

Weiner, P. K.; Kollman, P. A. (1981): Description of the AMBER program for molecular mechanics. *Journal of Computational Chemistry*, vol. 2, pp. 287–303.

Xie, G. Q.; Long, S. Y. (2006): Elastic vibration behaviors oof carbon nanotubes based on micropolar mechanics. *CMC: Computers, Materials & Continua*, vol. 4, no. 1, pp. 11–19.

Xie, G. Q.; X.Han; Long, S. Y. (2007): Characteristic of waves in a multi-walled carbon nanotube. *CMC: Computers, Materials & Continua*, vol. 6, no. 1, pp. 1–11.

Appendix A: The Newton-Raphson method

In statics and implicit dynamics, the Newton-Raphson method, also known as Newton's method, is the predominant technique for solving the system of nonlinear equations

$$\mathbf{R}(\overline{\mathbf{u}}) = \mathbf{0} \quad . \tag{67}$$

As a direct calculation of the solution vector

$$\overline{\mathbf{u}} = \mathbf{u} + \mathbf{c} \tag{68}$$

or the vector $\mathbf{c}$, which has to be added to a previously determined approximation $\mathbf{u}$, is not feasible, a Taylor series expansion

$$\mathbf{R}(\overline{\mathbf{u}}) = \mathbf{R}(\mathbf{u}) + D\mathbf{R}(\mathbf{u}) \cdot \mathbf{u} + \ldots \tag{69}$$

is performed which then is truncated after the linear term $D\mathbf{R}(\mathbf{u}) \cdot \mathbf{u}$:

$$D\mathbf{R}(\mathbf{u}) = \operatorname{grad} \mathbf{R} = \frac{d\mathbf{R}}{d\mathbf{x}} = \frac{d\mathbf{R}}{d\mathbf{u}} = \mathbf{K}_{\mathrm{T}} \quad . \tag{70}$$

In structural mechanics, $\mathbf{R}$ denotes the vector of the residual forces and $\mathbf{K}_{\mathrm{T}}$ the tangential stiffness matrix

$$K_{\mathrm{T},ij}(\mathbf{u}^k) = \left. \frac{\partial R_i}{\partial u_j} \right|_{\mathbf{u}^k} \tag{71}$$

with the degrees of freedom i and j. The solution vector $\mathbf{c}$ of the system of linear equations

$$\mathbf{K}_{\mathrm{T}}(\mathbf{u}^k)\cdot\mathbf{c} = -\mathbf{R}(\mathbf{u}^k) \tag{72}$$

has to be is added to the approximation of the previous iteration step k

$$\mathbf{u}^{k+1} = \mathbf{u}^k + \mathbf{c} \tag{73}$$

until increment $\mathbf{c}$ and residuum $\mathbf{R}$ are sufficiently small. Alternatively, an "energy norm" $\mathbf{R}\cdot\mathbf{c}$ can be computed, which may also be used to verify the quadratic convergence rate of the Newton-Raphson method

$$\frac{(\mathbf{R}\cdot\mathbf{c})^{k+2}}{(\mathbf{R}\cdot\mathbf{c})^{k+1}} \approx \left[\frac{(\mathbf{R}\cdot\mathbf{c})^{k+1}}{(\mathbf{R}\cdot\mathbf{c})^{k}}\right]^2 \tag{74}$$

in the vicinity of the solution.

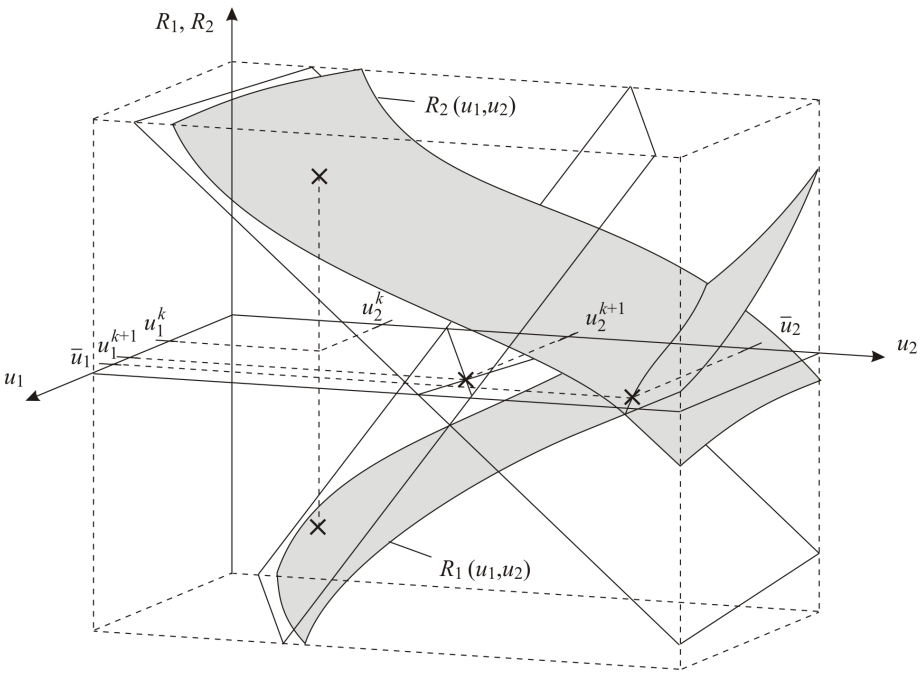

Figure 18: Illustration of Newton-Raphson method

To illustrate the Newton-Raphson method, Fig. 18 shows a system of two nonlinear equations $\mathbf{R} = \mathbf{0}$ or $(R_1, R_2) = (0,0)$ with the degrees of freedom u_1 and u_2. The

solution $\overline{\mathbf{u}} = (\overline{u}_1, \overline{u}_2)$ can be interpreted geometrically as the intersection point of the two planes $R_1 = R_1(u_1, u_2)$ and $R_2 = R_2(u_1, u_2)$ with the u_1-u_2-plane. For the solution, at first two tangential planes are constructed using the points $R_1(u_1^k, u_2^k)$ and $R_2(u_1^k, u_2^k)$ defined by the approximation $\mathbf{u}^k = (u_1^k, u_2^k)$ of the time increment k. The intersection point of the two planes with the u_1-u_2-plane yields a better approximation $\mathbf{u}^{k+1} = (u_1^{k+1}, u_2^{k+1})$ which then is used to start the next iteration step.

Appendix B: Stiffness matrices of MDFEM elements

A consistent linearization of the MDFEM elements introduced in section 4.2 is required to obtain a quadratic convergence rate of the Newton-Raphson method. For the 2-node element, the derivative of the nodal forces $\mathbf{F}_i$ with respect to the displacements $\mathbf{u}_j$ is obtained by means of the product rule

$$\frac{\partial \mathbf{F}_i}{\partial \mathbf{u}_i} = -\frac{\partial \mathbf{F}_i}{\partial \mathbf{u}_j} = -\frac{\partial \mathbf{F}_j}{\partial \mathbf{u}_i} = \frac{\partial \mathbf{F}_j}{\partial \mathbf{u}_j} = -\mathbf{n}_{ij} \otimes \frac{\partial F_{ij}}{\partial \mathbf{u}_i} - F_{ij} \frac{\partial \mathbf{n}_{ij}}{\partial \mathbf{u}_i} \tag{75}$$

with the derivatives of the unit vectors

$$\frac{\partial \mathbf{n}_{ij}}{\partial \mathbf{u}_i} = -\frac{\partial \mathbf{n}_{ij}}{\partial \mathbf{u}_j} = \frac{\mathbf{n}_{ij} \otimes \mathbf{n}_{ij} - \underline{\mathbf{1}}}{|\mathbf{x}_j - \mathbf{x}_i|} \tag{76}$$

and the derivatives of the force magnitudes. Depending on the chosen approach, we get

$$\frac{\partial F_{ij}^{\text{lin}}}{\partial \mathbf{u}_i} = -\frac{\partial F_{ij}^{\text{lin}}}{\partial \mathbf{u}_j} = -k_{ij} \mathbf{n}_{ij} \tag{77}$$

or

$$\begin{aligned} \frac{\partial F_{ij}^{\text{Morse}}}{\partial \mathbf{u}_i} = -\frac{\partial F_{ij}^{\text{Morse}}}{\partial \mathbf{u}_j} = -(2\alpha_{ij} n_{ij})^2 D_{ij} \big[& \exp(-2\alpha_{ij} n_{ij} (|\mathbf{x}_j - \mathbf{x}_i| - R_{ij}^0)) \\ & - 0.5 \exp(-\alpha_{ij} n_{ij} (|\mathbf{x}_j - \mathbf{x}_i| - R_{ij}^0)) \big] \mathbf{n}_{ij} \end{aligned} \tag{78}$$

for the chemical bonds and

$$\frac{\partial F_{ij}^{\text{LJ}}}{\partial \mathbf{u}_i} = -\frac{\partial F_{ij}^{\text{LJ}}}{\partial \mathbf{u}_j} = 12 \frac{D_{\text{ij,vdW}}}{\left(R_{\text{ij,vdW}}^0\right)^2} \left[-13 \left(\frac{|\mathbf{x}_j - \mathbf{x}_i|}{R_{\text{ij,vdW}}^0} \right)^{-14} + 7 \left(\frac{|\mathbf{x}_j - \mathbf{x}_i|}{R_{\text{ij,vdW}}^0} \right)^{-8} \right] \mathbf{n}_{ij} \tag{79}$$

for van der Waals bondings.

In case of the 3-node element, we obtain

$$\begin{aligned}
\frac{\partial \mathbf{F}_i}{\partial \mathbf{u}_a} &= \mathbf{n}_i \otimes \frac{\partial F_{ijk}}{\partial \mathbf{u}_a} + F_{ijk} \frac{\partial \mathbf{n}_i}{\partial \mathbf{u}_a} \\
\frac{\partial \mathbf{F}_k}{\partial \mathbf{u}_a} &= \mathbf{n}_k \otimes \frac{\partial F_{kji}}{\partial \mathbf{u}_a} + F_{kji} \frac{\partial \mathbf{n}_k}{\partial \mathbf{u}_a} \\
\frac{\partial \mathbf{F}_j}{\partial \mathbf{u}_a} &= -\frac{\partial \mathbf{F}_i}{\partial \mathbf{u}_a} - \frac{\partial \mathbf{F}_k}{\partial \mathbf{u}_a} \qquad \text{with} \quad a = i, j, k
\end{aligned} \tag{80}$$

as a function of

$$\begin{aligned}
\frac{\partial \mathbf{n}_i}{\partial \mathbf{u}_a} &= \mathbf{n}_{ij} \times \frac{\partial \mathbf{n}_{ijk}}{\partial \mathbf{u}_a} - \mathbf{n}_{ijk} \times \frac{\partial \mathbf{n}_{ij}}{\partial \mathbf{u}_a} \\
\frac{\partial \mathbf{n}_k}{\partial \mathbf{u}_a} &= \mathbf{n}_{jk} \times \frac{\partial \mathbf{n}_{ijk}}{\partial \mathbf{u}_a} - \mathbf{n}_{ijk} \times \frac{\partial \mathbf{n}_{jk}}{\partial \mathbf{u}_a} \qquad \text{with} \quad a = i, j, k
\end{aligned} \tag{81}$$

with

$$\begin{aligned}
\frac{\partial \mathbf{n}_{ijk}}{\partial \mathbf{u}_a} &= \frac{\frac{\partial (\mathbf{n}_{ij} \times \mathbf{n}_{jk})}{\partial \mathbf{u}_a} |\mathbf{n}_{ij} \times \mathbf{n}_{jk}| - (\mathbf{n}_{ij} \times \mathbf{n}_{jk}) \otimes \frac{\partial |\mathbf{n}_{ij} \times \mathbf{n}_{jk}|}{\partial \mathbf{u}_a}}{|\mathbf{n}_{ij} \times \mathbf{n}_{jk}|^2} \\
&= \frac{\left(\mathbf{n}_{ij} \times \frac{\partial \mathbf{n}_{jk}}{\partial \mathbf{u}_a} - \mathbf{n}_{jk} \times \frac{\partial \mathbf{n}_{ij}}{\partial \mathbf{u}_a} \right) - \mathbf{n}_{ijk} \otimes \mathbf{n}_{ijk} \left(\mathbf{n}_{ij} \times \frac{\partial \mathbf{n}_{jk}}{\partial \mathbf{u}_a} - \mathbf{n}_{jk} \times \frac{\partial \mathbf{n}_{ij}}{\partial \mathbf{u}_a} \right)}{|\mathbf{n}_{ij} \times \mathbf{n}_{jk}|} \\
&= \frac{\left(\underline{\mathbf{1}} - \mathbf{n}_{ijk} \otimes \mathbf{n}_{ijk} \right) \left(\mathbf{n}_{ij} \times \frac{\partial \mathbf{n}_{jk}}{\partial \mathbf{u}_a} - \mathbf{n}_{jk} \times \frac{\partial \mathbf{n}_{ij}}{\partial \mathbf{u}_a} \right)}{|\mathbf{n}_{ij} \times \mathbf{n}_{jk}|} \qquad \text{with} \quad a = i, j, k
\end{aligned} \tag{82}$$

and the derivatives of the magnitudes

$$\frac{\partial F_{ijk}^{\text{lin}}}{\partial \mathbf{u}_a} = \frac{K_{ijk}}{R_{ij}^0} \frac{\partial \Theta_{ijk}}{\partial \mathbf{u}_a} \quad \text{with} \quad a = i, j, k \tag{83}$$

or

$$\frac{\partial F_{ijk}}{\partial \mathbf{u}_a} = \begin{cases} \frac{C_{ijk}}{R_{ij}^0} \left[\cos \Theta_j^0 \cos \Theta_{ijk} - \cos(2\Theta_{ijk}) \right] \frac{\partial \Theta_{ijk}}{\partial \mathbf{u}_a} & \text{for } \Theta_j^0 \neq 180^\circ \\ -\frac{K_{ijk}}{R_{ij}^0} \cos \Theta_{ijk} \frac{\partial \Theta_{ijk}}{\partial \mathbf{u}_a} & \text{for } \Theta_j^0 = 180^\circ \text{ with } a = i, j, k \end{cases} \tag{84}$$

with

$$\frac{\partial \Theta_{ijk}}{\partial \mathbf{u}_a} = \frac{\mathbf{n}_{ij} \cdot \frac{\partial \mathbf{n}_{jk}}{\partial \mathbf{u}_a} + \mathbf{n}_{jk} \cdot \frac{\partial \mathbf{n}_{ij}}{\partial \mathbf{u}_a}}{\sqrt{1 - (\mathbf{n}_{ij} \cdot \mathbf{n}_{jk})^2}} \quad . \tag{85}$$

The derivatives $\frac{\partial \mathbf{n}_{ij}}{\partial \mathbf{u}_a}$ are given in Eq. 76. Note that the following derivatives vanish: $\frac{\partial \mathbf{n}_{ij}}{\partial \mathbf{u}_k} = \mathbf{0}$, if $k \neq i \wedge k \neq j$. The derivatives of the load magnitudes F_{ijk} and F_{kji} with respect to the displacements $\mathbf{u}_a$ depend on the lever arms and are related as follows:

$$\frac{\partial F_{kji}}{\partial \mathbf{u}_a} = \frac{\partial F_{ijk}}{\partial \mathbf{u}_a} \frac{R^0_{ij}}{R^0_{jk}} \quad . \tag{86}$$

For the 4-node torsion element, the computation of

$$\begin{aligned}
\frac{\partial \mathbf{F}_I}{\partial \mathbf{u}_a} &= \mathbf{n}_{IJK} \otimes \frac{\partial F_{IIJK}}{\partial \mathbf{u}_a} + F_{IIJK} \frac{\partial \mathbf{n}_{IJK}}{\partial \mathbf{u}_a} \\
\frac{\partial \mathbf{F}_L}{\partial \mathbf{u}_a} &= \mathbf{n}_{JKL} \otimes \frac{\partial F_{LJKL}}{\partial \mathbf{u}_a} + F_{LJKL} \frac{\partial \mathbf{n}_{JKL}}{\partial \mathbf{u}_a} \\
\frac{\partial \mathbf{F}_J}{\partial \mathbf{u}_a} &= \alpha_{JIJK} \frac{\partial \mathbf{F}_I}{\partial \mathbf{u}_a} + \frac{\alpha_{JJKL}}{\alpha_{LJKL}} \frac{\partial \mathbf{F}_L}{\partial \mathbf{u}_a} \\
\frac{\partial \mathbf{F}_K}{\partial \mathbf{u}_a} &= \alpha_{KIJK} \frac{\partial \mathbf{F}_I}{\partial \mathbf{u}_a} + \frac{\alpha_{KJKL}}{\alpha_{LJKL}} \frac{\partial \mathbf{F}_L}{\partial \mathbf{u}_a} \qquad \text{with} \quad a = I,J,K,L
\end{aligned} \tag{87}$$

requires the derivatives $\frac{\partial \mathbf{n}_{ijk}}{\partial \mathbf{u}_a}$ already given in Eq. 82. Note that $\frac{\partial \mathbf{n}_{IJK}}{\partial \mathbf{u}_L} = \mathbf{0}$ and $\frac{\partial \mathbf{n}_{JKL}}{\partial \mathbf{u}_I} = \mathbf{0}$. The derivatives of the nodal force magnitudes are given as

$$\frac{\partial F^{\text{lin}}_{IIJK}}{\partial \mathbf{u}_a} = -\frac{V_{IJKL} n^2_{JK}}{2R^0_{IJ} \sin\Theta^0_J} \frac{\partial \varphi_{IJKL}}{\partial \mathbf{u}_a} \quad \text{with} \quad a = I,J,K,L \tag{88}$$

or

$$\frac{\partial F_{IIJK}}{\partial \mathbf{u}_a} = -\frac{V_{IJKL} n^2_{JK}}{2R^0_{IJ} \sin\Theta^0_J} \cos\left[n_{JK}(\varphi_{IJKL} - \varphi^0_{JK})\right] \frac{\partial \varphi_{IJKL}}{\partial \mathbf{u}_a} \quad \text{with} \quad a = I,J,K,L \tag{89}$$

with

$$\frac{\partial \varphi_{IJKL}}{\partial \mathbf{u}_a} = \begin{cases}
+\dfrac{(\mathbf{n}_{IJK} \times \mathbf{n}_{JKL}) \frac{\partial \mathbf{n}_{JK}}{\partial \mathbf{u}_a} + \mathbf{n}_{JK} \left(\mathbf{n}_{IJK} \times \frac{\partial \mathbf{n}_{JKL}}{\partial \mathbf{u}_a} - \mathbf{n}_{JKL} \times \frac{\partial \mathbf{n}_{IJK}}{\partial \mathbf{u}_a} \right)}{\sqrt{1 - [(\mathbf{n}_{IJK} \times \mathbf{n}_{JKL}) \cdot \mathbf{n}_{JK}]^2}} \\
\quad \text{for} \ \ (\mathbf{n}_{IJK} \cdot \mathbf{n}_{JKL}) \geq 0 \\
-\dfrac{(\mathbf{n}_{IJK} \times \mathbf{n}_{JKL}) \frac{\partial \mathbf{n}_{JK}}{\partial \mathbf{u}_a} + \mathbf{n}_{JK} \left(\mathbf{n}_{IJK} \times \frac{\partial \mathbf{n}_{JKL}}{\partial \mathbf{u}_a} - \mathbf{n}_{JKL} \times \frac{\partial \mathbf{n}_{IJK}}{\partial \mathbf{u}_a} \right)}{\sqrt{1 - [(\mathbf{n}_{IJK} \times \mathbf{n}_{JKL}) \cdot \mathbf{n}_{JK}]^2}} \\
\quad \text{for} \ \ (\mathbf{n}_{IJK} \cdot \mathbf{n}_{JKL}) < 0 \quad .
\end{cases} \tag{90}$$

Note that the torsion angle $\varphi_{IJKL} = \varphi_{IJKL}(\mathbf{u}_I, \mathbf{u}_J, \mathbf{u}_K, \mathbf{u}_L)$ depends on the displacements of all four atoms involved.